Exploring Sources of Ice Crystals in Cirrus Clouds: Comparative Analysis of Two Ice Nucleation Schemes in CAM6

Kai Lyu[1], Xiaohong Liu[1], Bernd Kärcher[2]

[1]Department of Atmospheric Sciences, Texas A&M University, College Station, 77840, USA
[2]DLR Institut für Physik der Atmosphäre, Oberpfaffenhofen, Wessling, 82234, Germany

Correspondence to: Xiaohong Liu (xiaohong.liu@tamu.edu)

Abstract. Ice nucleation, a critical process in cirrus clouds, remains a challenge in global climate models. To enhance the understanding, a novel ice nucleation parameterization based on the Kärcher (2022) (K22) scheme is introduced into the NCAR Community Atmosphere Model version 6 (CAM6). To investigate ice formation in cirrus clouds, sensitivity tests are conducted to analyze three ice sources from orographic gravity wave (OGWs), convective detrainment, and turbulence. These tests employ both the K22 scheme and the default Liu and Penner (2005) (LP05) scheme. Model evaluation includes 6-year climatology and nudged simulations representing the Small Particles in Cirrus (SPARTICUS) and O2/N2 Ratio and CO2 Airborne Southern Ocean Study (ORCAS) campaigns.

Both schemes simulate that convection detrained and turbulence-induced ice crystals are concentrated in low- to mid-latitudes, whereas OGW-induced ice crystals are concentrated in mid- to high latitudes. Compared to the LP05 scheme, the K22 scheme generates a higher number of ice crystals. The simulated cloud microphysical properties using the K22 scheme align well with observations for orographic cirrus during the SPARTICUS campaign. In orographic cirrus over high terrains at mid- to high latitudes, both schemes identify OGW-induced ice crystals as the dominant ice source. However, due to distinct competition parameterizations, the K22 scheme exhibits less competition from minor ice sources (convection detrained and turbulence-induced). This underscores the significance of competition mechanisms within nucleation schemes for accurate cirrus clouds simulation. The application of two distinct nucleation schemes provides valuable insights into the dominant ice sources in cirrus clouds.

1. Introduction

Cirrus clouds play an important role in the Earth's radiation budget, thereby affecting the climate (Liou, 1986). These ice clouds can reflect solar radiation back to space, cooling the planet (Chen et al., 2024; Forster et al., 2023). They can also absorb terrestrial longwave radiation and thus warm the planet. The balance between these two opposite processes is greatly influenced by the microphysical properties of ice crystals in cirrus clouds and determines the net cloud radiative forcing. The representation of cirrus clouds in global climate models (GCMs) has been recognized as a key factor in understanding the climate change (Boucher et al., 2013).

Ice crystals in cirrus clouds originate from two main processes, detrainment from convective clouds and in-situ nucleation (Krämer et al., 2016; Muhlbauer, Ackerman, et al., 2014). Cirrus clouds are formed through convective detrainment when air containing ice crystals flows out of convective clouds, such as anvils. These clouds are usually associated with high ice number concentrations (> 100 L^{-1}) (Heymsfield et al., 2017).

Ice crystals in in-situ cirrus clouds, such as orographic cirrus over high terrains, are primarily nucleated by aerosols. There are two nucleation mechanisms: homogeneous freezing of solution droplets and heterogeneous nucleation on ice nucleating particles (INPs). Homogeneous nucleation requires higher supersaturation (> ~40-60 %) and lower temperatures (< -37 °C), typically resulting in high ice number concentrations (> 100 L^{-1}). In contrast, heterogeneous nucleation occurs at lower supersaturation and higher temperatures, involving INPs such as dust and black carbon (BC). This process generally produces low ice number concentrations (< 100 L^{-1}) (Froyd et al., 2022; Heymsfield et al., 2017).

Substantial progress has been made in understanding homogeneous nucleation (Koop et al., 2000). Homogeneous nucleation is usually triggered by high vertical velocities (> 0.1 m s^{-1}). These dynamic factors can be induced by either turbulence in the unstable circumstances with small Richardson numbers or gravity waves in the stable atmosphere with large Richarson numbers (Heymsfield et al., 2017).

Recent studies on cirrus clouds in GCMs usually overlook the roles of ice crystal sources, especially for cirrus clouds with high ice number concentrations (> 100 L^{-1}). The absence or misrepresentation of a critical ice source may lead to the failure to simulate cirrus cloud properties. For example, most GCMs treat turbulence as the sole subgrid-scale vertical velocity mechanism driving ice nucleation. However, research has shown that due to limitations in higher-order turbulence closure theory, cirrus clouds formed by gravity waves are usually absent in GCMs (Golaz et al., 2002b; Huang et al., 2020). Notably, studies have demonstrated that incorporating the effects of orographic gravity waves (OGWs) into ice nucleation processes enables models to successfully simulate the observed characteristics of orographic cirrus clouds (Lyu et al., 2023). In addition, many studies highlight that ice crystals from convective detrainment can have a significant impact on the microphysical properties of cirrus clouds, particularly in the tropical regions (Horner & Gryspeerdt, 2023; Horner & Gryspeerdt, 2024; Nugent et al., 2022). In this study, we focus on three ice sources: OGW-induced, turbulence-induced and convective detrained.

Aerosols such as dust, soot, metallic particles, and biological particles, can act as INPs, inducing heterogeneous nucleation and potentially suppressing homogeneous nucleation (Fan et al., 2016; Froyd et al., 2022; Heymsfield et al., 2017; Kärcher & Ström, 2003; Knopf & Alpert, 2023). The activation efficiency of INPs is determined by their chemical components, which is highly dependent on their sources (Beall et al., 2022; Chen et al., 2024; Tobo et al., 2019). Limited knowledge of the number concentration, chemical composition, and activation efficiency of INPs in the upper troposphere complicates the model prediction of cirrus clouds microphysical properties (Kärcher et al., 2022; Knopf & Alpert, 2023). Moreover, currently conventional GCMs cannot resolve the subgrid-scale vertical velocity, which drives the water vapor supersaturation for ice nucleation, posing additional uncertainty for model simulations.

Several parameterizations of nucleation mechanisms have been developed in GCMs. Liu and Penner (2005) (LP05) developed a parameterization that includes homogeneous nucleation, heterogeneous nucleation and their interactions. The parameterization was subsequently applied to the NCAR Community Atmospheric Model (CAM) (Liu et al., 2007) and was further refined to include the effects of pre-existing ice (Shi et al., 2015). A new parameterization (Kärcher, 2022), referred to as K22, that encompasses homogeneous nucleation, heterogeneous nucleation, their interactions, and competition with preexisting cirrus ice, has been integrated into CAM6. The purpose of this paper is to integrate the K22 nucleation parameterization into GCMs and evaluate its effects on cloud microphysical properties and dominant sources of ice crystals in cirrus clouds. Section 2 presents a description of the model, and the parameterization method used in the study. The observational data employed for evaluation are described in Section 3. The model results, along with comparisons to the default LP05 parameterization, are discussed in Section 4. Finally, the summary and conclusions are presented in Section 5.

2. Model and Parameterization

2.1 Model Description

The NCAR Community Atmosphere Model version 6 (CAM6) model is the atmosphere component of Community Earth System Model version 2 (CESM2) (Danabasoglu et al., 2020). CAM6 employs the updated Morrison-Gettelman cloud microphysics scheme (MG2) to predict the mass and number concentrations of cloud liquid, cloud ice, rain and snow (Gettelman & Morrison, 2015; Morrison & Gettelman, 2008). The deep convection processes are represented using the Zhang and McFarlane (1995) scheme. The planetary boundary layer turbulence, cloud macrophysics, and shallow convection are treated by the Cloud Layers Unified by Bi-normals (CLUBB) (Bogenschutz et al., 2013; Golaz et al., 2002a; Hinz et al., 1996). Aerosols are treated using the 4-mode version of Modal Aerosol Model (MAM4) (Liu et al., 2016). Since CLUBB effectively represents turbulence with a small Richardson number but struggles to produce perturbations caused by gravity waves (Golaz et al., 2002a, 2002b; Huang et al., 2020), subgrid-scale vertical velocities from orographic gravity waves (OGWs) and turbulence are incorporated into the ice nucleation schemes (Lyu et al., 2023). The turbulence-driven vertical velocity is derived from turbulence kinetic energy (TKE) calculated by CLUBB. Aerosols involved in ice nucleation act interactively with the MAM4. When new ice crystals form, the nucleated aerosols are transferred from the interstitial state to the cloud-borne state. Similarly, when cloud droplets form, the nucleated aerosols are transferred to the cloud-borne state and are subject to precipitation scavenging. The radiation calculations are based on the Rapid Radiative Transfer Model for General Circulation Models (RRTMG) (Iacono et al., 2008).

2.2 Ice Nucleation Parameterizations

2.2.1 K22 Scheme

In the K22 parameterization homogeneous freezing is treated as a stochastic process in which the number of activated solution droplets (n_{homo}) over time based on freezing rate (j) ($n_{homo} = \int j dt$). The freezing rate is determined using the liquid water volume (V) of the droplet population and a rate coefficient (J) derived from a water activity-based formula (Koop et al., 2000) ($j=VJ$). Vertical velocity (w), supersaturation with respect to ice (S_{i}), and temperature (T) significantly influence water activity ($J=J(w, S_{\mathrm{i}}, T)$) (Baumgartner et al., 2022; Kärcher et al., 2022; Liu & Penner, 2005). The scheme assumes a monodisperse liquid solution droplet distribution at a wet radius of 0.25 µm. The formulation of the number of ice crystals nucleated homogeneously is described by Kärcher et al. (2022).

For heterogeneous nucleation, a deterministic (time-independent) approach to predict the number (n) of activated INPs is employed in the K22 parameterization as follows:

$$n = n_{tot}\Phi(s), \tag{1}$$

where n_{tot} is the number concentration of INPs (e.g., coarse mode dust) and Φ is the activated INP fraction. Φ can be represented as either a linear ramp or a hyperbolic tangent function. Since we consider dust as the INPs, a linear ramp is applied in our study.

The function Φ can be expressed as follows:

$$\Phi = \begin{cases} 0 & : \ s < s_{min} \\ \frac{(s-s_{min})}{s_{max}-s_{min}} & : \ s_{min} \leq s \leq s_{max}, \\ 1 & : \ s > s_{max} \end{cases} \tag{2}$$

where s_{min} and s_{max} are two parameters that define the range of ice supersaturation where heterogeneous nucleation can occur. In our study, they are set to 0.22 and 0.3, respectively.

The equation governing the temporal evolution of ice supersaturation, s, in the ice-vapor system is expressed as

$$\frac{ds}{dt} = a(s+1)w - \int_0^s \frac{4\pi}{v n_{sat}} \frac{dn}{ds'} \left(\int_{\tau(s')}^{t(s)} r^2 \frac{dr}{dt} dt \right) ds' \ , \tag{3}$$

where $\frac{ds}{dt}$ represents the time derivative of s. The first term on the right-hand side of the equation is the production term related to adiabatic cooling. a is a thermodynamic parameter (Pruppacher et al., 1998) relating to adiabatic vertical air motion, and w is restricted to the updraft speed ($w > 0$). The second term signifies the loss term due to the removal of water vapor. The upper integration limit is the time t corresponding to ice supersaturation s, and the lower integration limit is a time τ corresponds to $0 \leq s' \leq s$.

Within the integral, r is the radius of spherical ice crystals, $\frac{dr}{dt}$ denotes the associated growth rate per ice crystal, v represents the volume of one water molecule in bulk ice, and n_{sat} is the water vapor number concentration in gas phase at ice saturation. The number concentration of ice crystals formed by INPs in a range of supersaturation ds' is given by $\frac{dn}{ds'}$.

The loss term in Equation (3) can be integrated numerically as described by Kärcher (2022). When $\frac{ds}{dt} = 0$, we can estimate the total heterogeneously nucleated ice number concentrations. Quenching velocities w_q are defined as:

$$w_q = \frac{\int_0^s \frac{4\pi}{v n_{sat}} \frac{dn}{ds'} \left(\int_{\tau(s')}^{t(s)} r^2 \frac{dr}{dt} dt \right) ds'}{a(s+1)}, \tag{4}$$

where the loss term includes contributions from heterogeneous nucleation and pre-existing ice. This approach allows us to determine an effective vertical updraft w_{eff} which is used to describe conditions relevant to the homogeneous nucleation.

The effective vertical updraft speed w_{eff} is calculated as:

$$w_{eff} = w - w_{q,het} - w_{q,pre}, \tag{5}$$

where w is the updraft speed, $w_{q,het}$ is the quenching velocity for ice crystals due to heterogeneous nucleation, and $w_{q,pre}$ is the quenching velocity due to pre-existing ice. If $w_{eff} \leq 0$, no homogeneous freezing occurs. When $w_{eff} > 0$, homogeneous nucleation will take place, but homogeneously nucleating ice number concentration will be smaller than that in the absence of INP-derived and pre-existing ice crystals (i.e. that calculated based on w) ($n_{homo} = n_{homo}(w_{eff})$).

2.2.2 LP05 Scheme

The LP05 ice nucleation scheme incorporates two primary mechanisms: homogeneous and heterogeneous nucleation (Liu & Penner, 2005). It is based on fitted simulation results from a cloud parcel model with varying vertical velocities. The maximum supersaturation is determined in the parcel model from the balance between the production due to adiabatic cooling by updrafts and loss due to vapor deposition on ice crystals. The number of nucleated ice crystals is derived based on ice supersaturation, temperature, aerosol number concentrations and composition, and vertical velocity. Subgrid-scale vertical velocity can be derived from TKE calculated by CLUBB, from OGWs, or from the combined contribution of both components.

Homogeneous nucleation in the LP05 scheme, similar to the K22 scheme, adopts the parameterizations by Koop et al. (2000). Sulfate aerosols in the Aitken mode with diameters greater than 0.1 μm is applied to fit to ice number concentrations (Gettelman et al., 2010). On the other hand, heterogeneous nucleation considers the coarse mode dust as potential source of INPs. The number of ice crystals formed due to heterogeneous nucleation n in the LP05 scheme is calculated using $n =$

$n_{dust} \cdot \Phi(T, w, S_i)$, where n_{dust} is the coarse mode dust number concentration from MAM4, and Φ is active aerosol fraction, empirically derived as a function of temperature (T), vertical velocity (w), and ice supersaturation (S_i).

The LP05 scheme considers the competition between homogeneous and heterogeneous nucleation. It determines the critical dust INP concentration, above which homogeneous nucleation is completely switched off. Below that homogeneous nucleation occurs partially and is gradually transitioned to the pure homogeneous nucleation at lower INP concentrations. The LP05 scheme is modified to consider the effect of pre-existing ice crystals (Shi et al., 2015), which is parameterized by reducing the vertical velocity for ice nucleation as a result of water vapor deposition on pre-existing ice.

2.2.3 Differences Between Two Schemes

The K22 scheme incorporates a physically-based competition of various ice sources grounded in a quasi-kinetic nucleation framework. It simulates the simultaneous evolution of both homogeneous and heterogeneous nucleation rates in response to changing supersaturation and aerosol properties. The framework allows a flexible parameterization of activation efficiencies of different INPs types. This approach explicitly tracks the kinetic interplay between pre-existing ice and different ice formation pathways, allowing for transient coexistence and interaction.

The LP05 scheme addresses the competition between nucleation mechanisms and pre-existing ice through an empirical framework derived from parcel model simulations. In this framework, supersaturation is implicitly partitioned, with the nucleation pathway most favorable under the given conditions being prioritized. Heterogeneous nucleation is favored at lower supersaturations and higher dust concentrations, while homogeneous nucleation predominates at higher supersaturations and lower dust concentrations. Pre-existing ice crystals are typically used as a threshold to judge whether new ice can be formed.

Overall, the K22 scheme provides a more continuous and interactive treatment of multiple ice nucleation pathways, with a stronger emphasis on the dynamic interplay between supersaturation, aerosol concentrations, and pre-existing ice crystals. On the other hand, the LP05 scheme employs a stepwise approach that directly compares the potential for nucleation with the concentration of pre-existing ice crystals, imposing a threshold when nucleation occurs. Uncertainties exist regarding the relationship between the reduction of supersaturation and the suppression of nucleation caused by pre-existing ice crystals. This relationship and its impact on the number of nucleated ice crystals requires further investigation.

The different strategies for representing ice nucleation pathways lead to stronger suppression of new ice formation in the LP05 scheme compared to the K22 scheme. In the LP05 scheme, competition between nucleation pathways is handled sequentially. Heterogeneous nucleation occurs first, followed by homogeneous nucleation only if the supersaturation exceeds a threshold (Liu & Penner, 2005). In addition, pre-existing ice crystals consume supersaturation before any new nucleation can occur (Kärcher et al., 2006; Shi et al., 2015), which further suppress new ice formation. In contrast, the K22 scheme represents homogeneous nucleation, heterogeneous nucleation, and pre-existing ice growth within a unified framework, allowing all processes to occur simultaneously. As a result, for example, when the number concentration of pre-existing ice crystals is high, the LP05 scheme strongly suppresses new ice formation due to its sequential competition approach. Meanwhile, the K22 scheme permits new ice formation by accounting for concurrent interactions among all ice-related processes, even under conditions where the LP05 scheme would inhibit nucleation.

2.3 Experiment Descriptions

The climatology experiments and nudged simulations related to the Small Particles in Cirrus (SPARTICUS) and O2/N2 Ratio and CO2 Airborne Southern Ocean Study (ORCAS) campaigns are designed and listed in Table 1 and 2. All simulations are conducted at a resolution of 0.9º × 1.25º with 56 vertical layers. We focus on the SPARTICUS and ORCAS campaigns in this study because they provide critical data on OGW-induced ice crystals. The SPARTICUS campaign involves flights over the mountainous regions from winter to summer, while the ORCAS campaign focuses on both ocean and continental regions during the summer.

In this study, the OGW experiments serve as the reference experiments. These experiments consider three primary sources of ice crystals: convective detrainment, nucleation driven by turbulence (CLUBB-TKE), and nucleation driven by OGWs. To isolate the effects of each source, we designed three sensitivity experiments: no_DET (no detrainment), no_TKE (no CLUBB-TKE) and no_OGW (no OGWs), each excluding one of these specific sources. By comparing the differences in ice number concentration (N_i) between the reference experiments and sensitivity experiments, we aim to understand the contribution of each ice source in CAM6.

Table 1 Description of 6-year Climatology Simulations

Model experiment	*Description*
LP05_OGW-Climo	Default CAM6 configuration with turbulence (CLUBB-TKE) and orographic gravity waves (OGWs) for ice nucleation.
LP05_no_OGW-Climo	Same as LP05_OGW-Climo but without OGWs for ice nucleation
LP05_no_DET-Climo	Same as LP05_OGW-Climo but without detrained ice.
LP05_no_TKE-Climo	Same as LP05_OGW-Climo but without turbulence for ice nucleation.
LP05_OGW-Homo-Climo	Same as LP05_OGW-Climo but only consider homogeneous ice nucleation.
LP05_OGW-Hete-Climo	Same as LP05_OGW-Climo but only consider heterogenous ice nucleation.
K22_OGW-Climo	Same as LP05_OGW-Climo but with K22 nucleation parameterization.
K22_no_OGW-Climo	Same as LP05_no_OGW-Climo but with K22 nucleation parameterization.
K22_no_DET-Climo	Same as LP05_no_DET-Climo but with K22 nucleation parameterization.
K22_no_TKE-Climo	Same as LP05_no_TKE-Climo but with K22 nucleation parameterization.
K22_OGW-Homo-Climo	Same as K22_OGW-Climo but only consider homogeneous ice nucleation.
K22_OGW-Hete-Climo	Same as K22_OGW-Climo but only consider heterogenous ice nucleation.
K22_OGW_Shan-Climo	Same as K22_OGW-Climo but with aerosol wet removal in convection (Shan et al., 2021).

Table 2 Description of Nudged Simulations

Model experiment	*Description*
2009 October to 2010 June	
LP05_OGW-SP	Default CAM6 configuration with turbulence and orographic gravity waves (OGWs) for ice nucleation.
LP05_no_OGW-SP	Same as LP05_OGW-SP but without OGWs for ice nucleation
LP05_no_DET-SP	Same as LP05_OGW-SP but without detrained ice.
LP05_no_TKE-SP	Same as LP05_OGW-SP but without turbulence for ice nucleation.
K22_OGW-SP	Same as LP05_OGW-SP but with K22 nucleation parameterization.
K22_no_OGW-SP	Same as LP05_no_OGW-SP but with K22 nucleation parameterization.
K22_no_DET-SP	Same as LP05_no_DET-SP but with K22 nucleation parameterization.
K22_no_TKE-SP	Same as LP05_no_TKE-SP but with K22 nucleation parameterization.
K22_OGW-Homo-SP	Same as K22_OGW-SP but only consider homogeneous ice nucleation.
K22_OGW-Hete-SP	Same as K22_OGW-SP but only consider heterogenous ice nucleation.
2015 October to 2016 February	
LP05_OGW-OR	Same as LP05_OGW-SP except simulation period.
LP05_no_OGW-OR	Same as LP05_no_OGW-SP except simulation period.
LP05_no_DET-OR	Same as LP05_no_DET-SP except simulation period.
LP05_no_TKE-OR	Same as LP05_no_TKE-SP except simulation period.
K22_OGW-OR	Same as K22_OGW-SP except simulation period.
K22_no_OGW-OR	Same as K22_no_OGW-SP except simulation period.
K22_no_DET-OR	Same as K22_no_DET-SP except simulation period.
K22_no_TKE-OR	Same as K22_no_TKE-SP except simulation period.

3. Observational Data

3.1 SPARTICUS campaign

This study utilizes observational data obtained during the SPARTICUS field campaign, conducted from January to June 2010 in the Central United States. The flight tracks of the campaign are depicted in Fig. 1a, covering approximately 150 research flight hours targeting cirrus clouds. Temperature measurements were conducted using the Rosemount probe Model

102 probe with a precision of ±0.5 ℃. Vertical velocity was measured by the Aircraft-Integrated Meteorological Measurement System-20 (AIMMS-20) instrument mounted on a Learjet 25 (Muhlbauer, Kalesse, et al., 2014). Ice crystals with diameters ranging from 10 to 3000 μm were measured using two-dimensional stereo-imaging probes (2D-S). The 2D-S probe minimizes biases in the number concentration of small-sized ice crystals by addressing ice shattering effects (Lawson, 2011). Observational data were sampled at a frequency of 1 Hz. A total of 6236 data samples are available in both observational and simulated datasets during the five days identified as orographic cirrus events (Muhlbauer, Ackerman, et al., 2014).

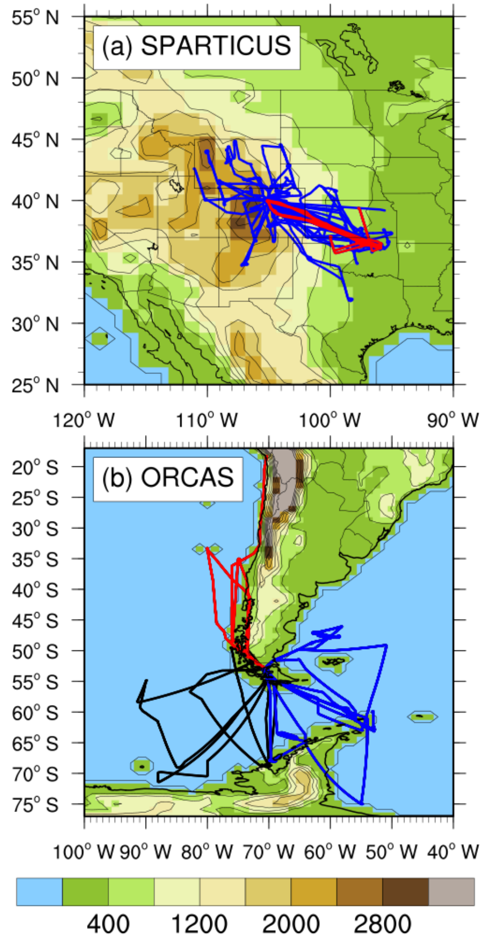

Figure 1. The top panel (a) shows aircraft trajectories (solid blue lines) during the SPARTICUS campaign. Solid red lines indicate flight tracks on days when orographic cirrus was observed (March 19, 30, April 1, 28, and 29, 2010). The bottom panel (b) shows aircraft trajectories during the ORCAS campaign. Color shading and black line contours illustrate the surface terrain (in m). Red lines denote flight tracks in Region 1, located north of Punta Arenas, Chile (SCCI), on the following days: January 23, and 25, February 8, 10, 17, 19, 22, 23 and 29, 2016. Blue lines denote flight tracks in Region 2, southeast of SCCI, on January 18, 25, and 30, February 12, 18, and 25, 2016. Black lines show flight tracks in Region 3, southwest of SCCI, on January 15, and 21, February 5 and 24, 2016.

At a speed of approximately 230 m s^{-1}, the aircraft covers about 100 km in 430 seconds of flight time, which corresponds to the model's horizontal resolution (1 degree). To facilitate a meaningful comparison between observational data and model outputs, a running average of 430 seconds of measurement data is applied (Patnaude et al., 2021). Additionally, the microphysical properties (such as ice number N_i, ice water content IWC and number-weighted diameter

D_{num}) of ice crystals with diameters larger than 20 µm from CAM6 results are derived using the size cut method described by Eidhammer et al. (2014), consistent with the measurements obtained by the 2D-Stereo Particle Probe (2D-S) but excluding the first size bin. Recent study suggests excluding the 2D-S probe's first size bin (5-15 µm) to avoid overestimating ice number concentration (Jensen et al., 2013; Mitchell et al., 2024). We adopt the midpoint of the second size bin (15 - 25 µm), i.e., 20 µm, as the size threshold (Lyu et al., 2023) because hydrometeors smaller than 25 µm cannot be fully recorded (Glienke & Mei, 2019). However, disregarding measurements for particles smaller than 20 µm may overlook certain signatures of homogeneous freezing. To address this, we also provide supplementary results that include ice crystals with diameters larger than 10 µm, offering a more comprehensive analysis.

3.2 ORCAS campaign

The O_2/N_2 Ratio and CO_2 Airborne Southern Ocean Study (ORCAS) was an NSF-sponsored airborne field campaign conducted from Chile during January and February 2016. The campaign utilized the NSF/NCAR HIAPER Gulfstream V (GV) aircraft for 18 flights over a period of 6 weeks. The data, sampled at 1 Hz, encompasses a total of 95 flight hours (Stephens et al., 2018). Ice cloud particles are measured by the Fast 2-Dimensional Optical Array Cloud probe (Fast-2DC), which detects particle sizes ranging from 62.5 to 1600 µm (excluding the first two bins due to the ice shattering effects). The primary difference in measuring ice properties between the SPARTICUS and ORCAS campaigns is the instrumentation used to measure ice crystals. The SPARTICUS campaign employs the Fast 2D-S probe, while the ORCAS campaign utilizes the 2D-C probe. Due to the ice shattering effect, the reliability of small ice measurements is compromised with the 2D-C probe. The subsequent paragraphs will delve into ice microphysical properties, specifically focusing on large-size ice crystals (D_{num} $\geq$ 62.5µm) observed during the ORCAS campaign.

The ORCAS flight profiles encountered a lot of samples of cold upper-tropospheric clouds. To derive the properties (such as N_i, IWC and D_{num}) of ice crystals with diameter $\geq$ 62.5 µm from CAM6 results, the size cut method described by Eidhammer et al. (2014) is employed. This methodology ensures consistency with the measurements obtained by the 2D-C probe (Section 3.1).

To better evaluate the model results, this study divides the ORCAS flights into three regions, as illustrated in Fig. 1b. Flights in Region 1 primarily traverse high mountain ranges where cirrus clouds form primarily due to OGWs, together with convection and frontal waves. Flights spanning Regions 2 and 3 predominantly cover oceanic areas, heavily influenced by convection and frontal waves. Notably, Region 2 is located downwind of the Andes Mountains and Antarctic high plateaus, thereby experiencing the additional influence from OGWs on observed cirrus cloud microphysical properties, while cirrus in Region 3 are less affected by OGWs.

This regional division allows for a more detailed analysis of cirrus cloud processes. The observed differences in cloud microphysical properties across these three regions highlight the distinct characteristics of cirrus clouds over land and ocean, particularly in mid- and high latitudes. These differences can provide insights into how various ice nucleation processes and environmental factors influence cirrus clouds formation and evolution.

4. Results

4.1 Climatology Experiments

Fig.2 illustrates the grid-mean ice number concentration (N_i) for different types of cirrus in climatology experiments using the LP05 and K22 schemes. The results indicate that N_i is generally higher in the K22_OGW-Climo experiment compared to the LP05_OGW-Climo experiment. In both schemes, ice crystals detrained from convection are primarily concentrated in the tropical regions and mid-latitudes, and in situ nucleated ice crystals induced by turbulence are prevalent near the tropical tropopause layers (TTL) and in mid-latitudes. In contrast, due to the presence of mountains and high plateaus, orographic cirrus due to OGWs are concentrated over mid- and high latitudes. Across all three ice sources, experiments based on the K22 scheme produce higher ice number concentrations than those based on the LP05 scheme, mainly from the OGW-induced cirrus.

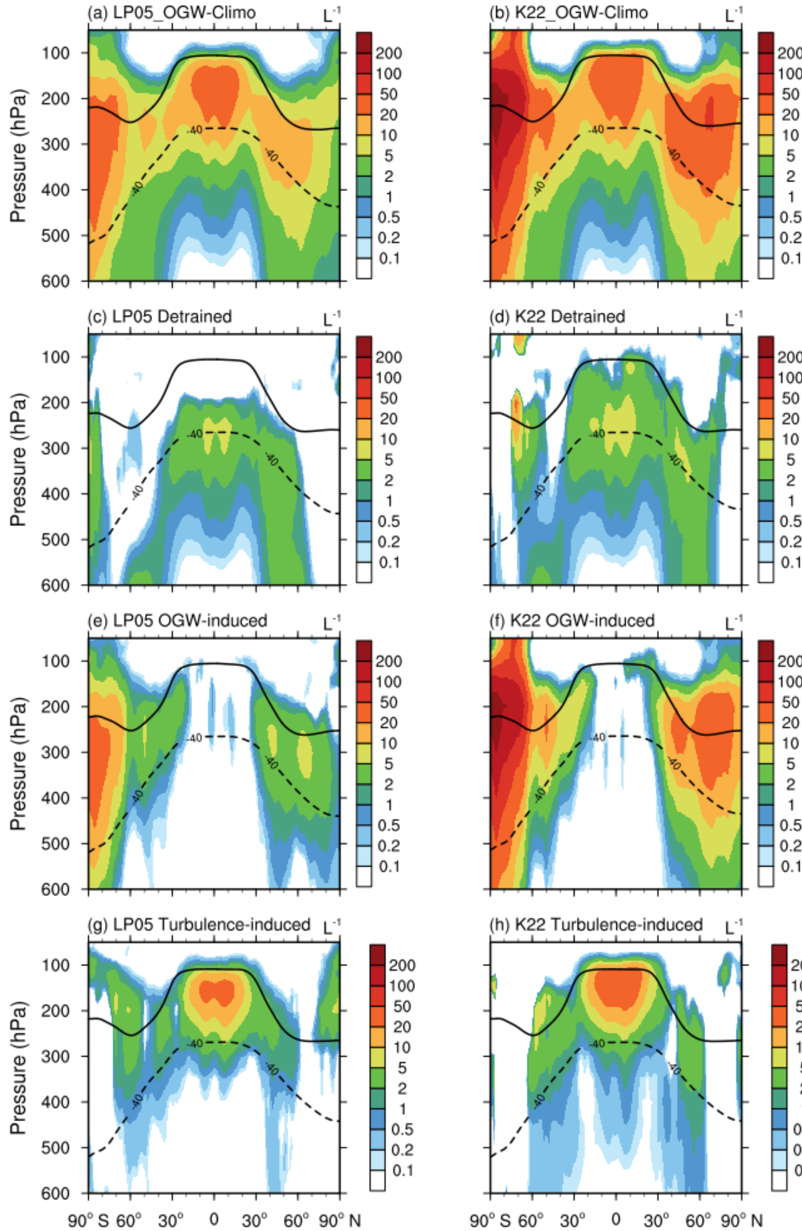

Figure 2. Annual zonal grid-mean ice number concentration (N_i) from 6-year climatology simulations in the upper troposphere (above 600 hPa). The first row shows N_i from the LP05_OGW-Climo and K22_OGW-Climo experiments. The second row shows the differences in N_i between OGW and no_DET experiments (OGW – no_DET) for both the LP05 and K22 schemes, highlighting the contribution from cirrus clouds associated to convective detrainment. The third row presents the N_i differences between OGW and no_OGW experiments (OGW – no_OGW) for both schemes, indicating the presence of orographic cirrus. The fourth row presents the N_i differences between OGW and no_TKE experiments (OGW – no_TKE) for both schemes, reflecting cirrus clouds formed due to turbulence. Dashed lines represent the annual mean -40°C isothermal line, while solid lines indicate the tropopause in the corresponding simulations.

We further analyze grid-mean N_i in the sensitivity tests using homogeneous-only and heterogeneous-only experiments (shown in Fig. 3). These experiments include OGW-induced, turbulence-induced and detrained sources of ice crystals. The results reveal that both nucleation processes produce more ice crystals in the K22 scheme compared to the LP05 scheme. In addition, the N_i resulting from the OGW-Climo experiments in both the K22 and LP05 schemes closely resembles those from their corresponding OGW-Homo-Climo experiments. This similarity indicates that homogeneous nucleation is a major contributor to the nucleated ice number globally in both the LP05_OGW-Climo and K22_OGW-Climo experiments.

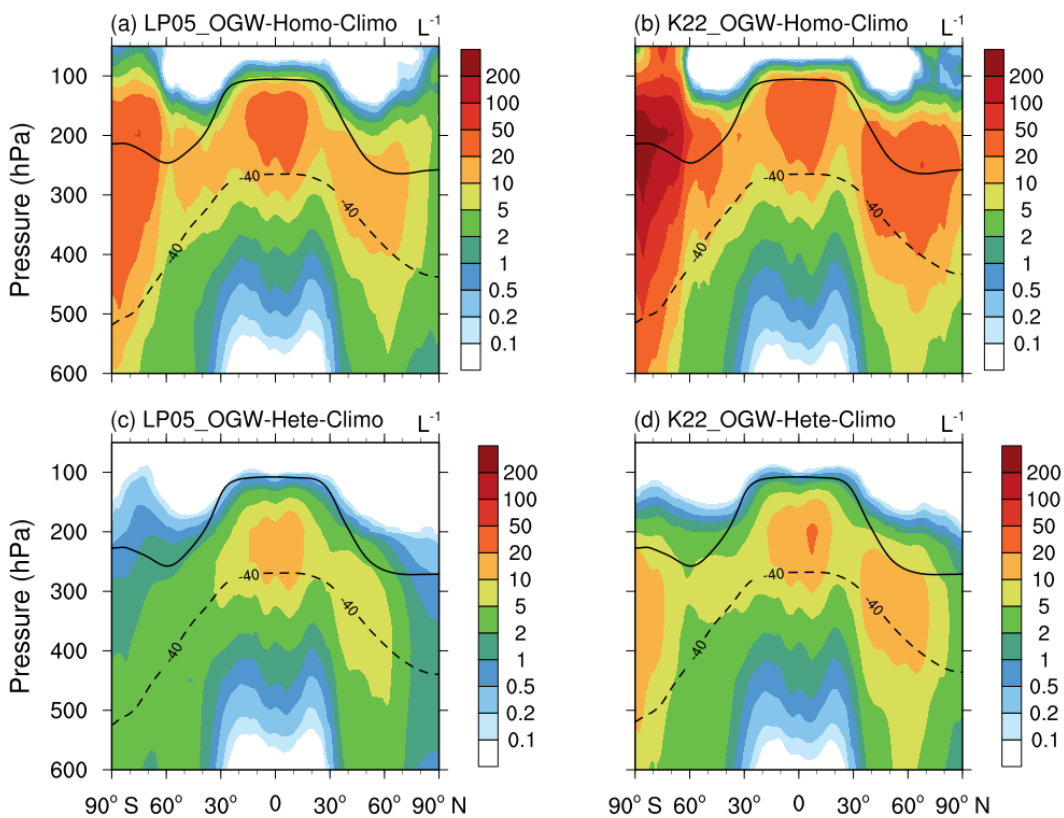

Figure 3. Annual zonal grid-mean N_i from 6-year Climatology simulations in the upper troposphere (above 600 hPa). Dashed lines indicate the annual mean -40 °C isothermal line, and solid lines represent the tropopause in the corresponding simulations.

The K22 scheme simulates higher activated number concentrations of aqueous aerosols for homogeneous nucleation compared to the LP05 scheme, as shown in Fig. 3a, b. This difference can be attributed to both direct and indirect influences. The direct effect stems from how each scheme represents the competition of nucleated with pre-existing ice crystals. As described in Section 2.2.3, the number of nucleated ice crystals in the LP05 scheme tends to be more suppressed by the competition with pre-existing ice, compared to the K22 scheme. Consequently, the presence of pre-existing ice crystals leads to fewer ice crystals that are formed, producing overall lower ice number concentrations in the LP05 scheme. The indirect effects are associated with differences in temperatures and vertical velocity fields between the two schemes.

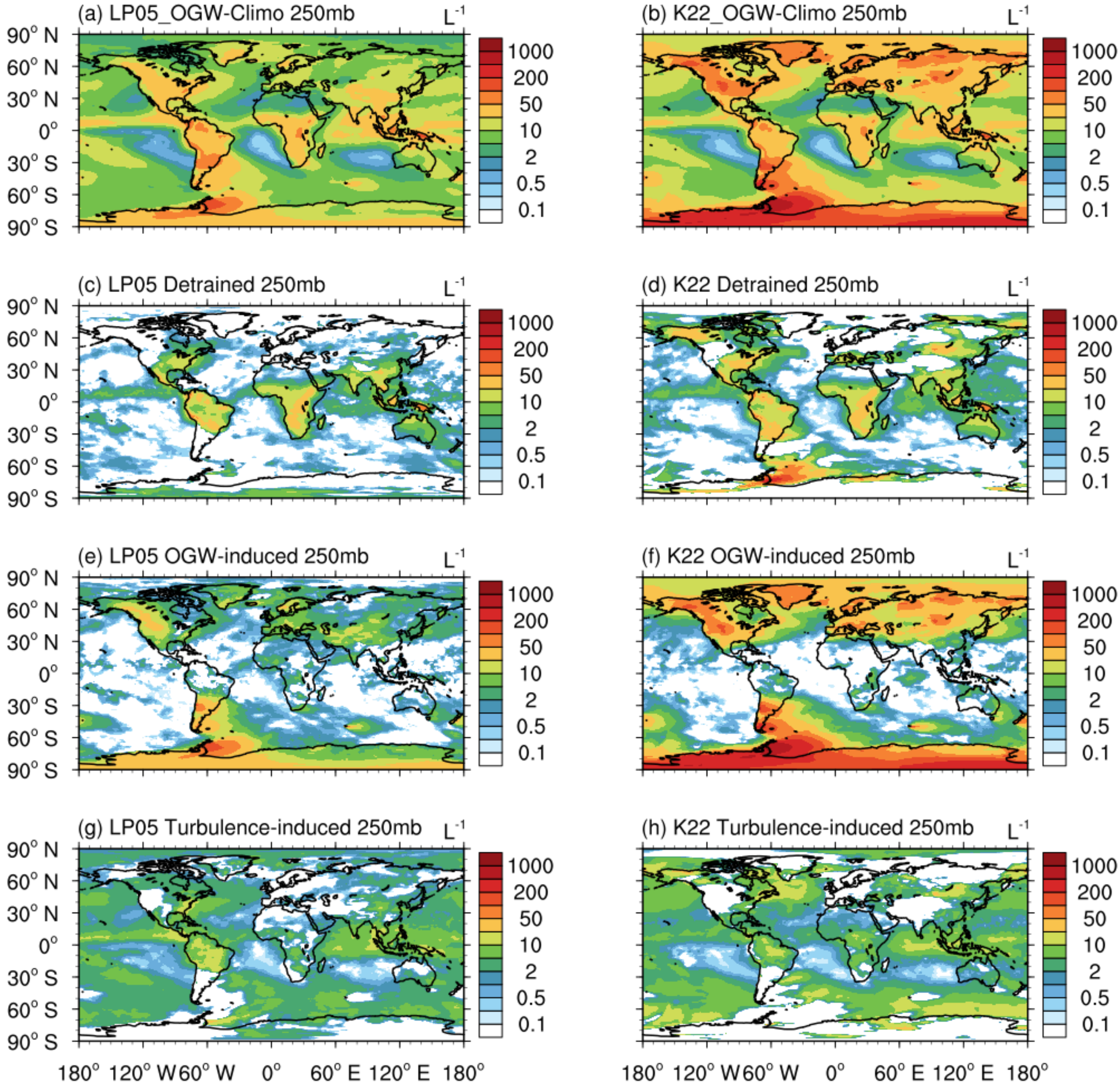

Figure 4. Annual grid-mean N_i from 6-year climatology simulations at 250 hPa. The first row shows N_i from the LP05_OGW-Climo and K22_OGW-Climo experiments. The second row shows the differences in N_i between OGW and no_DET experiments (OGW – no_DET) for both the LP05 and K22 schemes, highlighting the contribution from cirrus clouds associated to convective detrainment. The third row presents the N_i differences between OGW and no_OGW experiments (OGW – no_OGW) for both schemes, indicating the presence of orographic cirrus. The fourth row presents the N_i differences between OGW and no_TKE experiments (OGW – no_TKE) for both schemes, reflecting cirrus clouds formed due to turbulence.

Fig. 4 shows the global longitude-latitude distribution of annual mean N_i at 250 hPa. In both schemes, cirrus clouds related to convective detrainment are frequently simulated over land in low and mid-latitudes, while cirrus clouds due to OGWs primarily occur over mountains and highlands in mid- and high latitudes. Turbulence-induced cirrus clouds exhibit widespread global coverages. Consistent with the results shown in Fig. 2, the K22_OGW-Climo experiment produces higher N_i values in all three cirrus types compared to the LP05_OGW-Climo experiment (Fig. 4a and 4b). While the distribution of detrained N_i appears similar in low latitudes between the two schemes, notable differences emerge in high latitudes, with the K22 scheme generating more ice crystals, particularly over Alaska and the Antarctic Peninsula (Fig. 4c and 4d). OGW-induced ice crystals in the K22 scheme are more abundant and broadly distributed over mountainous regions compared to the LP05 scheme (Fig. 4e and 4f). Additionally, the K22 scheme simulates a higher number of turbulence-induced ice crystals, especially over mid- and high latitude regions (Fig. 4g and 4h). For OGW-induced cirrus clouds, the K22 scheme distributes high N_i values (>100 L^{-1}) more extensively than the LP05 scheme, particularly in mid- and high latitudes. This broader distribution results in a higher cloud frequency in the K22 scheme, as shown in Fig. S1.

To analyze the factors driving differences in N_i between the LP05 and K22 schemes, several key variables should be considered. These factors include temperature, which affects ice nucleation thresholds and saturation vapor pressure; subgrid-scale vertical velocity, which determines the supersaturation necessary for ice formation; and dust aerosol number concentration, along with the fraction of activated INPs (Φ), which together determine the number of heterogeneously nucleated ice crystals.

In high latitudes, temperature increases in the upper troposphere are found in the K22_OGW-Climo experiment compared to the LP05_OGW-Climo experiment (Fig. S2), likely due to localized warming associated with increased cirrus cloud occurrence (Fig. S1). However, these temperature changes are generally small (typically smaller than ±0.25 °C) and mostly positive, suggesting a suppression of ice nucleation. Therefore, the impact of temperature difference on global N_i is expected to be negative and unlikely to account for a globally significant increase in N_i observed in the K22 scheme (Fig. 2).

Similarly, subgrid-scale vertical velocity increases in the K22_OGW-Climo experiment compared to the LP05_OGW-Climo experiment, particularly in the upper troposphere at mid- and high latitudes (Fig. S3). While these changes may enhance ice nucleation locally, their overall impact on N_i remains limited, as vertical velocity changes are generally small (less than ±0.002 m s^{-1}) in most regions. Therefore, they are unlikely to explain the globally significant increase in N_i simulated in the K22 scheme (Fig. 2).

The most substantial differences in N_i between the two schemes arise from microphysical processes, particularly those governing heterogeneous ice nucleation. Both the K22 and LP05 schemes account for the activation of coarse mode dust particles, but the K22 scheme simulates higher dust aerosol number concentrations, especially in the upper troposphere (Fig. S4). This enhancement is likely driven by changes in large scale circulation patterns and surface wind fields resulting from differences in the applied ice nucleation schemes, which influence both dust emission and atmospheric transport. As a result, the K22 scheme shows an increase in ice number concentration nucleated from dust particles heterogeneously, as shown in Fig. 3c and 3d. The activated INP fraction Φ also plays a crucial role in controlling heterogeneous nucleation. While Φ depends on local thermodynamic conditions, such as temperature, vertical velocity, and supersaturation in the LP05 scheme, the K22 scheme simplifies this dependence, with Φ relying on supersaturation only. Differences in the treatment of Φ, combined with elevated dust concentrations in the K22 scheme influence heterogeneous nucleation on coarse mode dust. However, since the number of coarse mode dust is limited (~10-30 L^{-1}) in the upper troposphere (Fig. S4), even if all the dust particles are nucleated heterogeneously to form ice crystals, their contribution to increased N_i will not reach the levels (~100 L^{-1}) observed in the K22 scheme. Therefore, these factors are unlikely to explain the globally significant increase in N_i seen in the K22 scheme compared to the LP05 scheme (Fig. 2a and Fig. 2b). This also implies that competition between preexisting ice and new ice nucleation is a more dominant factor influencing the simulated N_i.

Fig. S5 and Fig. S6 show the annual mean ice number tendency due to heterogeneous nucleation (ΔN_{i_het}) from 6-year climatology simulations, shown as zonal means (Fig. S5) and at 250 hPa (Fig. S6). Both schemes simulate ΔN_{i_het} are concentrated at mid- and high-latitudes in the upper troposphere (Fig. S5a, b), indicating that heterogeneous nucleation is most active in these regions. High ΔN_{i_het} values extend over land and ocean regions (Fig. S6a, b). Compared to the LP05 scheme, the K22 scheme simulates higher ΔN_{i_het} values in mid and high latitude regions. This enhancement aligns with the higher coarse mode dust number in the K22_OGW-climo experiment (Fig. S4). Both schemes show similar ΔN_{i_het} distributions from convective detrainment between no_DET and OGW experiments (Fig. S5c, d and Fig. S6 c, d), indicating that heterogeneous nucleation is not directly influenced by convective detrainment. In contrast, the no_OGWs experiments

(Fig. S5e, f and Fig. S6e, f) show pronounced reduction in ΔN_{i_het} in the mid- and high latitudes compared to OGW experiments, revealing the significant role of OGWs in enhancing heterogeneous nucleation. This effect is especially evident in the K22 scheme, which shows substantial ΔN_{i_het} reductions over continental regions, especially over mountainous areas such as the Himalayas, Andes, Alps and Rockies, indicating a strong sensitivity of heterogeneous ice nucleation to OGWs. The LP05 scheme exhibits more limited changes in ΔN_{i_het}, suggesting a weaker enhancement from OGWs. These different results between the two schemes are due to their distinct parameterizations of heterogeneous nucleation. For turbulence-induced ΔN_{i_het} (Fig. S5 g, h and Fig. S6g, h), both the K22_noTKE and LP05_noTKE experiments simulate reduced ΔN_{i_het} compared to their respective OGW-Climo experiments. This result indicates that turbulence reinforces INP activation.

Fig. S7 and Fig. S8 present the zonal mean and 250 hPa ice number tendency due to homogeneous nucleation (ΔN_{i_hom}). In both schemes, homogeneous nucleation primarily occurs over high mountains in mid- and high latitudes, as well as in the tropical tropopause layers (TTL). Overall, the K22 scheme produces larger ΔN_{i_hom} compared to LP05. The LP05_no_DET-Climo experiment exhibits enhanced ΔN_{i_hom} in the tropopause (Fig. S7c and S8c), compared to the LP05_OGW-Climo experiment, indicating that convective detrainment suppresses homogeneous nucleation in the LP05 scheme. In contrast, the K22_no_DET-Climo experiment exhibits limited changes compared to the K22_OGW-Climo experiment (Fig. S7d and S8d), indicating that detrainment has a limited effect on homogeneous nucleation in the K22 scheme. Both schemes simulate significantly reduced ΔN_{i_hom} over high mountains compared to the OGW experiments (Fig. S7e, f and S8e, f), emphasizing the role of OGWs in promoting homogeneous nucleation. Similarly, the no_TKE experiments (Fig. S7g, h and S8g, h) produce reduced ΔN_{i_hom} in the TTL for both schemes, revealing that turbulence enhances homogeneous nucleation in this region.

Further insight into the role of aerosol processes in ice nucleation is provided by the K22_OGW_Shan-Climo experiment, which incorporates an improved treatment of aerosol wet removal by convections based on Shan et al. (2021). In this configuration, dust aerosol concentrations are reduced due to more efficient convective scavenging (Fig. S9), particularly in convectively active low latitude regions. The resulting lower dust number concentrations lead to a reduced heterogeneous nucleation rate (Fig. S10 and S11), which can increase the homogeneous nucleation rate due to less competition from heterogeneous nucleation on dust (Fig. S10 and S11). In this case, improvements in aerosol wet removal may help optimize upper tropospheric aerosol concentrations and can leads to a general increase in N_i (Fig. S12).

When the ice nucleation scheme is switched from LP05 to K22, grid-averaged N_i increases in the mid- and high latitudes (Fig. S13a). Ice water content (IWC) also increases (Fig. S13b) especially over high mountains. Ice effective radius (AREI) over land tends to be smaller and AREI over ocean tends to be larger, compared to the LP05 scheme (Fig. S13c). In mid- and high latitudes, longwave cloud forcing (LWCF) is increased over high mountains, as can be seen in Fig. S13d. These changes can be explained by changes in the N_i (Fig. S13h), as the K22 scheme generally simulates more ice crystals over high mountains. Interestingly, negative LWCF can be found over oceans at mid- and high latitudes. This phenomenon is primarily associated with the dominance of optically thin cirrus clouds formed via in-situ nucleation in these regions, as previously reported (Sassen & Cho, 1992; Sassen et al., 2008; Wang et al., 1996; Winker & Wielicki, 2010). The K22 scheme tends to enhance the spatial extent and occurrence frequency of such clouds. Over oceans, where vertical velocities are weaker than over land, these optically thin clouds become even thinner. This allows more longwave radiation to space, resulting in negative LWCF over oceans, consistent with the previous findings (Muri et al., 2014; Spang et al., 2024). Shortwave cloud forcing (SWCF) increases in mid- and high latitudes (Fig. S13e), as the shortwave albedo of extensive cirrus clouds (10-40%) is lower than that of the underlying surface (ranging from 50-80% for oceans at low solar angles and 80-90% for snow-covered land). Changes in SWCF, LWCF and net cloud forcing (net CF) caused by the switch of ice nucleation scheme is -0.51 W m^{-2}, 2.95 W m^{-2}, and 2.44 W m^{-2}, respectively. The change in the cloud radiative forcing may influence global temperature, which can modify large-scale circulation and sub-grid turbulence, subsequently affect ice nucleation, cloud frequency, and cloud radiative forcing, and have important implications for high cloud feedbacks (Murray & Liu, 2022).

4.2 SPARTICUS Experiments

Fig. 5a presents the simulated N_i in orographic cirrus during the SPARTICUS campaign for both the LP05_OGW-SP and K22_OGW-SP experiments. Together with simulated IWC and D_{num} (Fig. S14), both schemes produce results that generally agree with observational data. The simulated IWC and N_i in the K22_OGW-SP experiment tend to be larger, while D_{num} tends to be smaller, compared with the LP05_OGW-SP experiment. This suggests that the K22 scheme simulates more, but smaller ice crystals. Fig. 5b shows the differences in simulated N_{i} between the reference experiments (OGW) and sensitivity experiments (no_OGW, no_DET and no_TKE). Larger differences in simulated N_{i} between sensitivity experiments and the reference experiments indicate a more significant contribution from a respective ice crystal source (OGW-induced, detrained, or turbulence-induced). Specifically, increase or decrease of microphysical properties in the sensitivity experiments compared to the reference experiments reveals how each source contributes to enhancing or inhibiting the overall ice number concentrations.

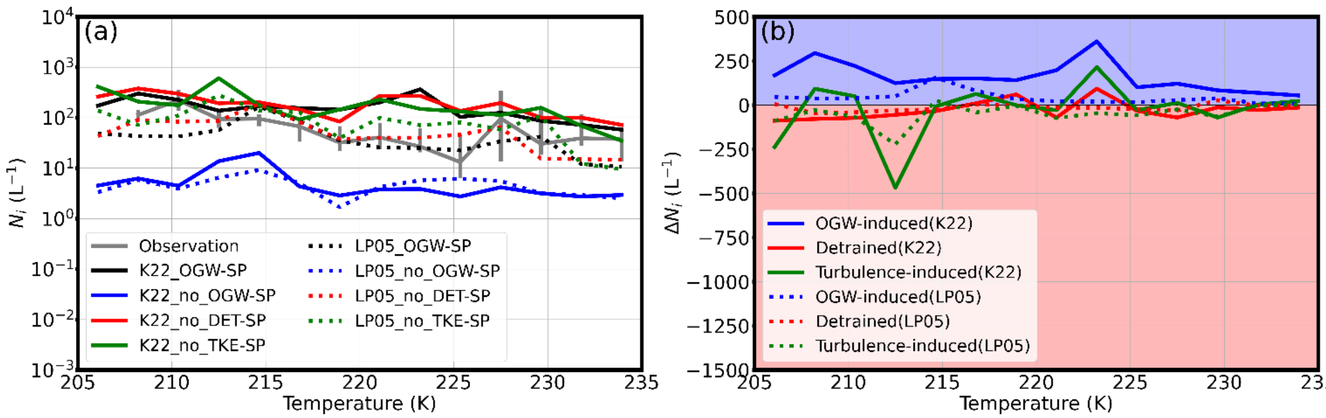

Figure 5. (a) Comparison of N_{i} between observations and experiments and (b) differences in median N_{i} values (ΔN_{i}) between sensitivity tests (no_OGW, no_DET and no_TKE) and reference experiments (OGW) in LP05 and K22 schemes during the SPARTICUS campaign. In panel (a), solid lines represent median N_{i} values from K22 experiments, while dotted lines represent those from LP05 experiments. The bars indicate observed N_{i} values, ranging from the 25th percentile to the 75th percentile. In panel (b), the number of ice crystals due to OGW is calculated as N_{i} in OGW experiments minus N_{i} in no_OGW experiments. The number of ice crystals from convection detrainment is calculated as N_{i} in OGW experiments minus N_{i} in no_DET experiments. The number of ice crystals due to turbulence is calculated as N_{i} in OGW experiments minus N_{i} in no_TKE experiments. The blue shaded region indicates that the ice crystal source contributes to N_{i} and increases N_{i} in the reference experiments. The red shaded region indicates that the ice crystal source competes with other sources and inhibits N_{i} in the reference experiments.

Fig. 5b shows that in both LP05 and K22 schemes, the changes in N_{i} (ΔN_{i}) due to OGWs are always positive and larger than those from the other two sources in these cirrus clouds. This indicates that OGWs play a significant role in enhancing the formation of ice crystals in cirrus clouds identified as orographic cirrus during the observed five-days period. Particularly in regions with temperatures below 215 K, where both schemes simulate their highest N_{i} peaks, ΔN_{i} due to OGWs peaks positively at the corresponding temperatures. This suggests that OGW-induced ice crystals enhance the overall N_{i} in these cirrus clouds. Detrained and turbulence-induced ΔN_i values show different signs, fluctuating between positive and negative at different temperatures, indicating that the effects of the other two sources are uncertain and vary between the two schemes. In the LP05 scheme, detrained and turbulence-induced ΔN_i values are generally negative, suggesting that ice crystals from both detrainment and turbulence tend to inhibit N_i. In contrast, the K22 scheme exhibits varied signs of detrained and turbulence-induced ΔN_i values, with stronger fluctuations between positive and negative, indicating that these sources can either enhance or inhibit N_i. .Notably, the positive ΔN_i values in detrained and turbulence-induced ice crystals are smaller in the LP05 scheme, suggesting stronger competition (inhibition effects) between ice sources in the LP05 scheme.

Regarding the simulated number weighted diameter of ice crystals (D_{num}) in the LP05 and K22 experiments (Fig. S15 and S16), the no_OGW experiments produce the largest D_{num} among all experiments. This implies that ice crystals nucleated due to OGW tend to have the smallest D_{num} in the simulations, highlighting the dominance of small, nucleated ice crystals from OGWs.

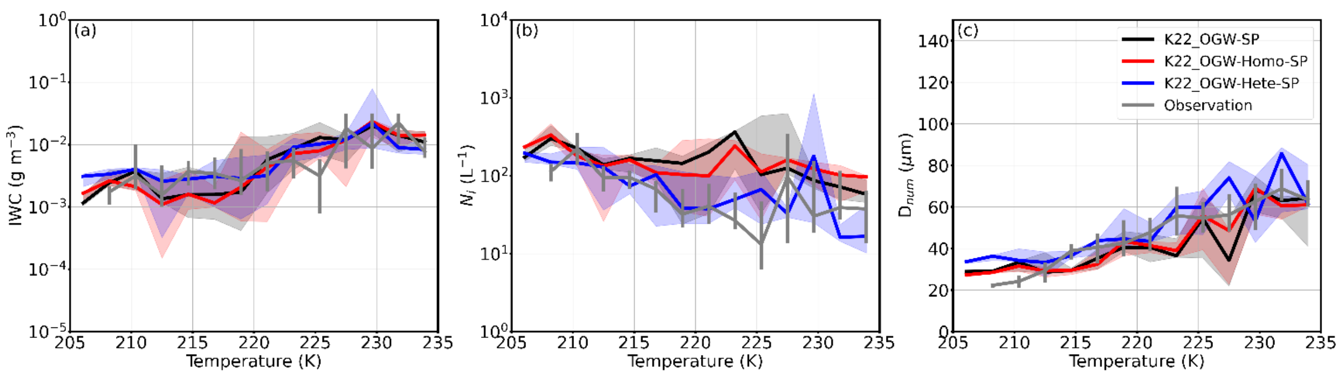

Figure 6. Comparison of IWC (a), N_i (b) and D_{num} (c) with respect to temperature between observations and K22 sensitivity experiments (K22_OGW, K22_OGW-Homo-SP and K22_OGW-Hete-SP) for orographic cirrus (5 days) during the SPARTICUS campaign.

A detailed analysis of sensitivity tests with the K22 scheme for simulating orographic cirrus clouds has been conducted. As depicted in Fig. 6, the microphysical properties (IWC, N_i and D_{num}) in the K22_OGW-SP experiment closely align with those in the K22_OGW-Homo-SP experiment. This similarity suggests that homogeneous nucleation is the dominant mechanism for orographic cirrus during the SPARTICUS campaign using the K22 scheme. This finding is consistent with the results of Lyu et al. (2023) using the LP05 scheme, who also identified the homogeneous nucleation as the dominant mechanism for ice nucleation in orographic cirrus during the SPARTICUS campaign. The simulated coarse mode dust number concentrations are shown in Fig. S17, which shows higher values in the K22 scheme than those in the LP05 scheme. However, the dust concentrations are very low (<1 L^{-1}) in both schemes, which supports the dominance of homogeneous nucleation for cirrus cloud formation during the SPARTICUS campaign.

Furthermore, comparing simulation results with observations, the microphysical properties in the K22_OGW-Hete-SP experiment show closer agreement with the observations than those in the other two experiments (Figure 6). This is largely due to the use of a 20-μm size cut threshold, which filters out many small ice crystals typically associated with homogeneous nucleation. This interpretation is supported by the 10-μm size cut results (Fig. S18), where the inclusion of data from the less reliable first size bin captures more small ice crystals, characteristic of homogeneous nucleation, leading to better agreement of D_{num} between observations and the K22_OGW-Homo-SP and K22_OGW-SP experiments. Additionally, discrepancies between the simulations and observations may stem from limitations in model representations of other microphysical processes, such as ice depositional growth, cloud ice to snow autoconversion, and accretion, and ice sedimentation.

4.3 ORCAS Experiments

In Region 1, both simulated and observed median values of IWC are typically low, around 10^{-3} g m^{-3}, implying that less water vapor is available for ice formation. The dataset used in the analysis includes 83559 data points. As shown in Fig. 7, the median simulated N_i generally hover around 3 L^{-1}, which is close to the upper limit of observed N_i range. However, simulated N_i tends to be overestimated, except near 225 K, where they are slightly underestimated compared to observations. The simulated coarse mode dust number concentrations are presented in Fig. S19, which shows higher values with the K22 scheme compared to the LP05 scheme.

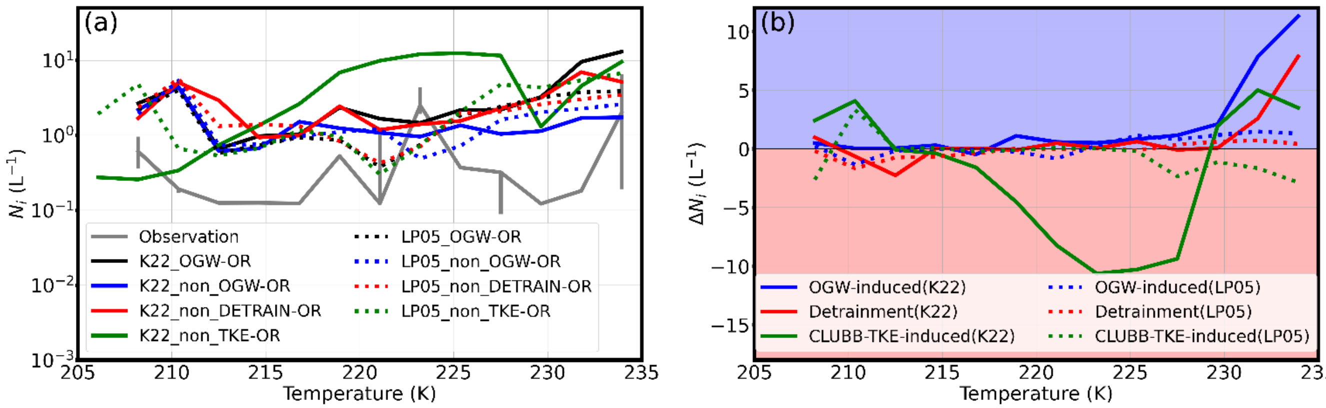

Figure 7. Same as Figure 5 but for cirrus clouds during the ORCAS campaign in Region 1.

As shown in Fig. 7, multiple observed N_{i} peaks correspond to different contributors to ΔN_{i}, revealing that cirrus clouds exhibit multilayer structures with distinct ice sources. Simulated N_{i} displays pronounced peaks above 225 K and near 210 K. At lower altitudes, where high N_{i} values are observed at temperatures above 225 K, both schemes simulate positive ΔN_{i} values, indicating that ice crystals due to OGWs and detrainment are the dominant contributors to simulated N_{i} in both schemes. In the LP05 scheme, turbulence-induced ΔN_{i} values are generally negative, implying that ice crystals from turbulence tend to suppress the overall N_{i}. In contrast, in the K22 scheme, turbulence-induced ΔN_{i} values fluctuate from negative to positive, suggesting inhibition between 215-230 K and enhancement at temperatures ≥ 235 K. At the 210 K level, the overwhelmingly positive ΔN_{i} values due to turbulence in both schemes suggest that turbulence-induced ice crystals are the primary contributor to N_{i} (Fig. 7b). However, in the LP05 scheme, ΔN_{i} values due to OGWs are negative, suggesting that OGW-induced ice crystals tend to inhibit ice crystal formation. In contrast, their impacts are minimal (~0) in the K22 scheme. In addition, both schemes simulate generally negative ΔN_{i} values due to detrainment, implying that detrained ice crystals tend to suppress the following ice formation.

Region 2, located downwind of the southern end of South America and the Antarctic peninsula, features a narrow landmass extending into the sea. These highlands create unique conditions for cirrus clouds, characterized by high vertical velocities. The dataset used in the analysis includes 146139 data points. The observed median IWC values in Region 2 remain close to 10^{-2} g m^{-3}, indicating a relatively moist environment. Figure S20 shows the simulated coarse mode dust number concentrations, with the K22 scheme generally simulating higher dust concentrations compared to the LP05 scheme.

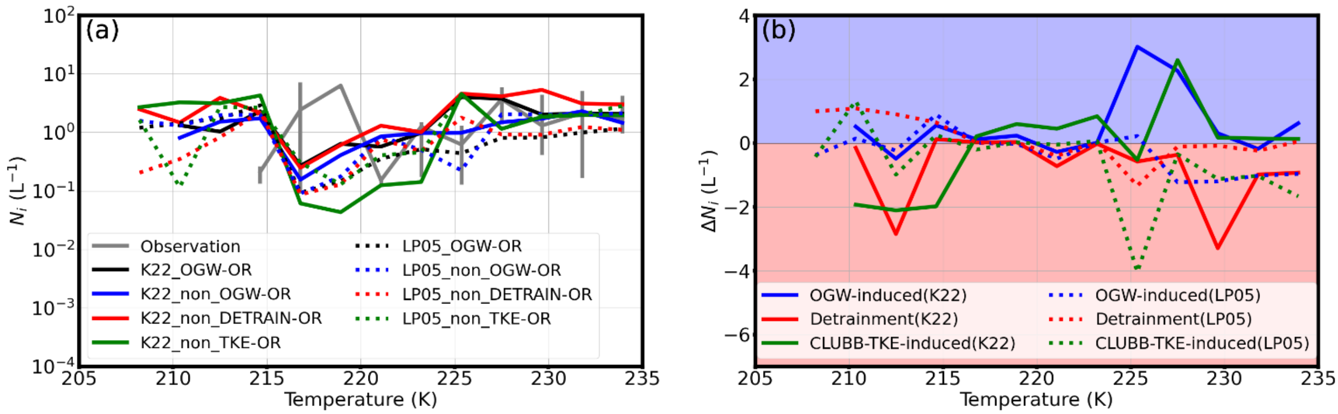

Figure 8. Same as Figure 7 except in Region 2.

In Fig. 8a, similar to Region 1, multiple high N_i peaks again correspond to different primary ΔN_i contributors, suggesting multilayer structures of cirrus clouds in Region 2. Near 215 K, the OGW experiments in both schemes simulate high N_i peaks that closely match the observed peak near 218 K. The corresponding positive OGW-induced ΔN_i values in both schemes (Fig. 8b) suggest that a large portion of these ice crystals are generated by OGWs originating from mountains and high plateaus. The contributions from other sources (detrainment and turbulence) differ between the two schemes. In the LP05 scheme, generally positive detrained ΔN_i and fluctuating turbulence-induced ΔN_i near 215K suggest an enhancement role from detrainment and a mix of enhancement and inhibition effects from turbulence. In contrast, the K22 scheme exhibits negative ΔN_i values for both sources, indicating overall inhibition effects. These findings imply that the N_i peaks around 215 K are strongly related to the mountainous terrain upwind of Region 2. Notably, while simulated N_i peaks are around 215 K, the observed N_i peak occurs around 219 K. This bias may be due to an underestimation of ice crystal fall speeds in the model, potentially caused by slow growth of simulated ice crystals or biases in the fall speed parameterization. The broader spatial distribution of ice crystals in the K22 scheme leads to stronger competition among multiple ice sources. In contrast, in the LP05 scheme, OGW-induced ice crystals tend to remain concentrated over mountainous areas (as shown in Fig. 4), resulting in more localized effects. In the K22 scheme, however, the high N_i (>100 L^{-1}) extends over a larger area, facilitating interaction and competition between OGW-induced ice sources and other ice sources, even far from the mountainous regions.

In the lower part of cirrus clouds (T > 225K), negative ΔN_i values of all three ice crystal sources in the LP05 scheme suggest universal competition among these sources. In contrast, in the K22 scheme, only detrained ΔN_i values are negative, suggesting inhibition effects, while ΔN_i values from OGWs and turbulence are positive, suggesting enhancement effects. The fact that no ΔN_i values from a single source are overall positive in both schemes may suggest that the dominant ice source is missing from the model. Previous studies have highlighted the importance of additional ice nucleation sources, such as frontal gravity waves, in the cirrus formation over oceans, and identified crucial INPs including dust, metallic particles, soot and biological materials (Fan et al., 2016; Froyd et al., 2022; Heymsfield et al., 2017; Kärcher & Ström, 2003; Knopf & Alpert, 2023). However, in CAM6, only OGWs are included in the ice nucleation, and only coarse mode dust is considered as INPs. In addition, other important N_i source and sink processes, such as secondary ice production, ice sublimation and sedimentation should be examined. Future studies are therefore necessary to incorporate these potential dynamic and microphysical sources to improve simulations of cirrus clouds over oceanic regions.

In Region 3, the observed median IWC values are even higher than those in Region 2, with maximum values reaching up to 10^{-1} g m^{-3}. This suggests a water vapor-rich environment for cirrus clouds in this region. There are 111712 data points used in the analysis. Multiple high N_i peaks with different primary contributors reveal multilayer structures of cirrus clouds, similar to Regions 1 and 2 (Fig. 9). Simulated coarse mode dust number concentrations from both schemes are compared in Fig. S21, showing that the K22 scheme simulates much higher dust concentrations than the LP05 scheme.

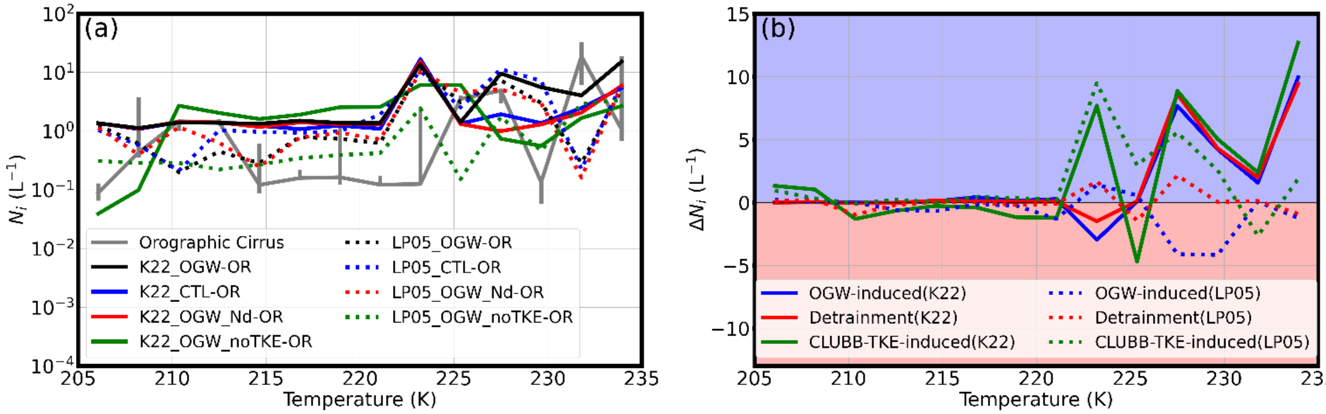

Figure 9. Same as Figure 7 except in Region 3.

In higher-level cirrus clouds (T < 220 K), both simulated and observed median N_i values are low, typically less than 1 L^{-1}. However, the simulated N_i in both schemes shows poor agreement with observations. This discrepancy may result from the inability of the model to capture the realistic dynamic factors necessary for ice nucleation (Gasparini et al., 2023; Kärcher & Podglajen, 2019). The absence of observed ice sources in the simulation points to potentially missing dynamic factors, such as frontal or convective gravity waves, which are likely key drivers of ice nucleation under these conditions. At low temperature levels (T < 209 K), both schemes exhibit positive turbulence-induced ΔN_i values, suggesting that ice crystals due to turbulence make the most contribution to N_i at these cold temperatures (Fig. 9b).

In the lower levels of cirrus clouds (T > 227 K), most of the simulated N_i peaks occur (Fig. 9a). At these temperatures, turbulence-induced ΔN_i values are mostly positive and generally exceed OGW-induced and detrained ΔN_i values in both schemes, suggesting a strong enhancement of N_i from turbulence. However, OGW-induced and detrained ΔN_i values differ between the two schemes. In the K22 scheme, positive OGW-induced and detrained ΔN_i values suggest significant enhancements to N_i from OGWs and detrainment. In contrast, the LP05 scheme shows large variability, with OGW-induced and detrained ΔN_i values fluctuating between positive and negative, indicating more complex and varied effects from these ice sources in the simulations.

Numerous studies have demonstrated that turbulence from CLUBB-TKE can hardly predict perturbations from gravity waves (Golaz et al., 2002a, 2002b; Huang et al., 2020). To accurately simulate cirrus clouds over oceans in Region 3, it is necessary to incorporate representations of other key dynamic drivers for ice nucleation, such as frontal and convective gravity waves. It is also important to incorporate key INPs (e.g., marine organic aerosols) besides mineral dust into ice nucleation schemes. Other source and sink terms beyond ice nucleation, such as secondary ice production, ice sublimation, and sedimentation, may also play a significant role in influencing the N_i evolution over oceans.

4.4 Implication of different behaviours in ice sources with the two nucleation schemes

Both K22 and LP05 schemes can effectively simulate the ice nucleation as a dominant ice source in orographic cirrus clouds, though they exhibit different influences from minor ice sources on simulated N_i. In both schemes, OGW-induced ice crystals emerge as the dominant contributors, while detrained and turbulence-induced ice crystals show varying effects as minor ice sources. This distinction is useful to identify cirrus types observed during the flight campaigns. To test this method, we identify orographic cirrus clouds during the SPARTICUS campaign by examining cases where OGW-induced ice source dominates in the simulations and the simulated N_i aligns closely with observations in both schemes. This analysis yields 16 such flight days: January 26, 27, February 10, 17, 19, 20, March 14, 17, 19, 30, April 1, 11, 12, 19, 28, and 29. Among these days, 5 days (March 19, 30, April 1, 28 and 29) correspond to previously identified orographic cirrus events reported by Muhlbauer, Ackerman, et al. (2014).: By expanding the previously identified orographic cirrus days, the number of available data points increases from 6236 to 15454, thereby enhancing robustness and credibility of our analysis.

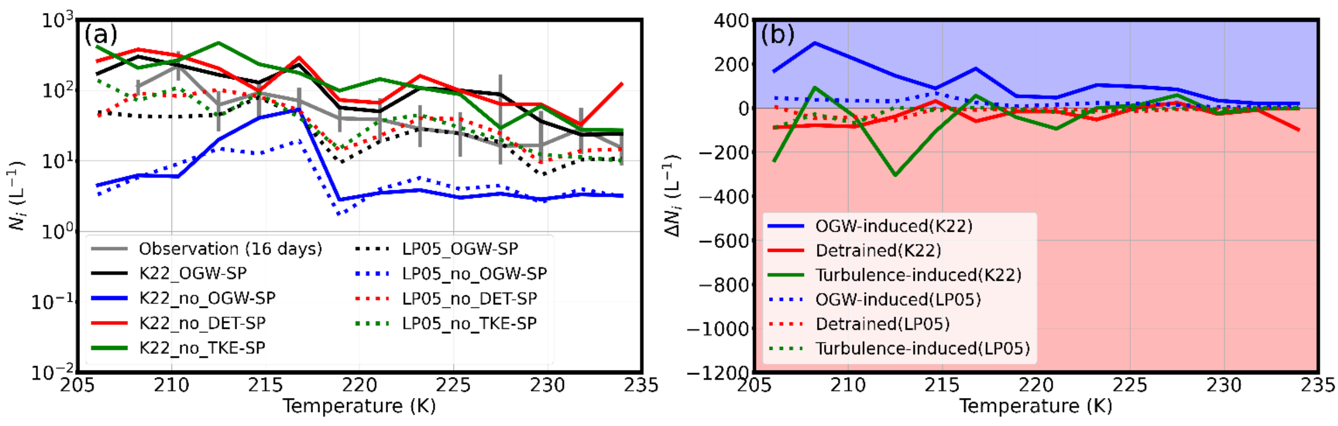

Figure 10. Same as Figure 5 except for identified orographic cirrus by our approach (16 days of flights).

Fig. 10 illustrates the microphysical properties of identified orographic cirrus over the 16-day period using our approach. Both schemes simulate N_i values that are in reasonable agreement with the observations. The N_i values in K22_OGW-SP experiment are generally larger than those in the LP05_OGW-SP experiment, while the observed N_i values fluctuate between these two simulations (Fig. 10a). The K22_OGW-SP experiment shows better agreement with observations at specific temperature levels (T ~ 210 K, ~220 K, and >230 K), while the LP05_OGW-SP experiment performs better at T~215K and ~225K. The positive OGW-induced ΔN_i values in both schemes suggest that OGW-induced ice crystals are the dominant contributors to N_i during these 16 days (Fig. 10b). These findings demonstrate that our method is effective and provides a reliable method to distinguish orographic cirrus in flight campaigns.

A comparison between results using a 20 µm size cut (Figs. 5, 6 and 10) and those using a 10 µm size cut (Figs. S18, S22 and S23) reveals that the observed N_i values decrease significantly when transitioning from the 10 µm to the 20 µm threshold. This reduction is because the concentration of ice crystals in the first size bin (5 – 15 µm) is significantly higher than those in subsequent larger bins, often dominating the total ice concentration (Jensen et al., 2013; Mitchell et al., 2024). Despite this decrease, OGW-induced ice crystals consistently remain the dominant contributor to total N_i. This consistency suggests that key signatures of homogeneous freezing are preserved across the two size thresholds, reinforcing robustness of our approach for identifying orographic cirrus clouds. Previous studies have highlighted that N_i in the first size bin (5 – 15 µm) measured by 2D-S probes may overestimate ice number concentrations (Jensen et al., 2013; Mitchell et al., 2024). Interestingly, the K22_OGW-SP experiment aligns closely with the observed N_i using the 10 µm size cut (Figs. S18, S22 and S23), potentially suggesting an overestimation of N_i in the K22 scheme. However, this interpretation remains uncertain without more reliable measurements on small ice crystals.

5. Summary and Conclusions

This study compares the newly introduced K22 ice nucleation scheme with the default LP05 ice nucleation scheme in the NCAR CAM6 model. The K22 scheme accounts for homogeneous nucleation, heterogeneous nucleation, their interactions, and competition with pre-existing ice. To investigate sources of ice crystals in cirrus clouds, we conduct six-year climatology simulations, with a focus on the effects of OGWs on ice nucleation. Additionally, nudged experiments are performed for the SPARTICUS and ORCAS flight campaigns to further compares the two ice nucleation schemes. In all simulations, coarse mode dust is considered as the sole INPs.

In the six-year climatology experiments, the K22_OGW-Climo experiment shows an increase in grid-mean N_i compared to the LP05_OGW-Climo experiment. Ice crystals detrained from convection are concentrated in low and mid-latitudes, while those formed due to OGWs are concentrated in mid- and high latitudes. Ice crystals due to turbulence are concentrated in low and mid-latitudes. Notably, homogeneous nucleation plays an important role in the global contribution to the total number of nucleated ice crystals.

The increase in nucleated ice numbers in the K22 scheme compared to the LP05 scheme can be attributed to both direct and indirect reasons. The direct reason lies in their different assumptions of treating the competition between pre-existing ice and nucleated ice crystals. The K22 scheme emphasizes the dynamic interplay between supersaturation, aerosol concentrations and pre-existing ice, allowing homogeneous nucleation, heterogeneous nucleation and the growth of pre-existing ice crystals to occur simultaneously. In contrast, the LP05 scheme is based on an empirical framework that favors a specific nucleation pathway. In the LP05 scheme, heterogeneous nucleation is favored at low supersaturation and high INP concentrations, while homogeneous nucleation dominates at high supersaturations. Pre-existing ice crystals consume supersaturation before new ice nucleation can occur. This may result in a stronger competition in the LP05 scheme, suppressing homogeneous nucleation.

The indirect reason is related to the increase in ice number concentrations within the K22 scheme, which appears to lead to higher cloud frequency. This can be due to the presence of smaller ice crystals in the K22 scheme, which have lower fall speeds, allowing them to travel over broader regions before completely sublimated. An increase in cloud frequency may induce changes in global temperature, potentially affecting turbulence and subgrid-scale vertical velocity, thereby impacting ice nucleation. However, these factors are not the key factors that cause the significant increase in N_i. In addition, the global increase in coarse mode dust concentrations leads to a higher number of heterogeneously nucleated ice crystals. However, improved aerosol wet removal parameterization due to convection can mitigate this effect by reducing the concentration of coarse mode dust in the upper troposphere.

The nudged experiments conducted during the SPARTICUS flight campaign specifically focus on orographic cirrus clouds. The K22_OGW-SP experiment generates microphysical properties comparable to those of the LP05_OGW-SP experiment, with both aligning reasonable with observational data. However, the K22_OGW-SP experiment tends to produce a higher number of smaller ice crystals compared to the LP05_OGW-SP experiment. Both the LP05 and K22 schemes identify OGWs as the dominant ice crystal source in orographic cirrus clouds observed during SPARTICUS, but the LP05 scheme exhibits greater competition from detrainment and turbulence sources than the K22 scheme. In addition, the K22_OGW-SP experiment simulates homogeneous nucleation as the dominant mechanism in orographic cirrus formation.

The ORCAS flight campaign is used to further evaluate the simulation results for both the K22 and LP05 schemes. Due to instrument limitations in measuring ice crystals, 2D-C probes are utilized during the ORCAS campaign, providing reliable observations of the microphysical properties of large-size ice crystal ($D_{num} \geq 62.5\mu m$). To better evaluate the results, the flight data is divided into three regions. Region 1 encompasses flights over high mountains, while Regions 2 and 3 cover flights mostly over oceans. Region 2, located downwind of the Andes Mountains and high plateaus in Antarctic, is also affected by orographic cirrus clouds, which impact the observed cloud microphysical properties.

Moreover, distinguishing ice crystal sources has long posed a significant challenge in the study of cirrus clouds. The different behaviours between dominant and minor ice sources with the K22 and LP05 schemes provide a reasonable method for identifying cirrus cloud types in observations, particularly orographic cirrus. Applying this method to the SPARTICUS campaign, we identify 16 flight days during which OGW-induced ice source dominates the ice formation, with no significant bias of N_i in either scheme. These selected flights exhibit reasonable agreement in microphysical properties with observations, proving that this method is effective for distinguishing orographic cirrus from observations.

Furthermore, our comparison between simulated cirrus clouds with observations highlights the need for refining the model representation of key processes governing cirrus cloud evolution. They include ice crystal growth (ice deposition and accretion), secondary ice production, sublimation, and ice crystal sedimentation. Differences in moisture availability and dynamic conditions between land and ocean also may lead to distinct cloud microphysical behaviors, resulting in unique cirrus cloud characteristics across these regions. Over land, particularly in mountainous regions, strong vertical velocities induced by mountains create favourable conditions for homogeneous ice nucleation, which often becomes the dominant nucleation mechanism in orographic cirrus clouds. In contrast, over oceans, the scarcity of strong vertical velocity sources in the upper troposphere over oceans results in heterogeneous nucleation being the prevailing nucleation mechanism. We note that other critical INPs (such as black carbon, metallic particles, biological materials) besides mineral dust are not currently represented in ice nucleation schemes (Lin et al., 2025). Further studies should also consider incorporating additional dynamic processes, such as frontal and convective gravity waves (Yook et al., 2025). In addition to gravity waves, uncertainties in the representation of other drivers of ice sources, such as turbulence and convective detrainment, should be reduced. Recent incorporations of convective cloud microphysics in deep convection (Lin et al., 2021; Song & Zhang, 2011) should help to reduce the uncertainty in detrained ice properties. Further evaluations of the K22 scheme based on model climatology will be conducted by comparing modelled cirrus with regional observational datasets (Krämer et al., 2016; Krämer et al., 2020) and global satellite data (Lyu et al., 2023).

Code and data availability. For readers interested in replicating specific aspects of our study, we encourage them to contact the corresponding authors of the cited papers for access to the underlying code and data.

Author contributions. KL: incorporated K22 scheme into CAM6, conducted simulations, analyzed results, wrote the article; XL: provided guidance, reviewed the manuscript; BK: provided K22 nucleation parameterization and reviewed the manuscript.

Competing interests. At least one of the (co-)authors is a member of the editorial board of Atmospheric Chemistry of Physics.

Disclaimer. Publisher's note: Copernicus Publications remains neutral with regard to jurisdictional claims made in the text, published maps, institutional affiliations, or any other geographical representation in this paper. While Copernicus Publications makes every effort to include appropriate place names, the final responsibility lies with the authors.

Acknowledgement. This work was supported by the National Aeronautics and Space Administration (NASA) grant (No. ROSES-2020 80NSSC21K1457).

Financial support. This research has been supported by the National Aeronautics and Space Administration (NASA) grant (No. ROSES-2020 80NSSC21K1457).

References

Baumgartner, M., Rolf, C., Grooß, J. U., Schneider, J., Schorr, T., Möhler, O., Spichtinger, P., & Krämer, M. (2022). New investigations on homogeneous ice nucleation: the effects of water activity and water saturation formulations. *Atmos. Chem. Phys.*, *22*(1), 65-91. https://doi.org/10.5194/acp-22-65-2022

Beall, C. M., Hill, T. C. J., DeMott, P. J., Köneman, T., Pikridas, M., Drewnick, F., Harder, H., Pöhlker, C., Lelieveld, J., Weber, B., Iakovides, M., Prokeš, R., Sciare, J., Andreae, M. O., Stokes, M. D., & Prather, K. A. (2022). Ice-nucleating particles near two major dust source regions. *Atmos. Chem. Phys.*, *22*(18), 12607-12627. https://doi.org/10.5194/acp-22-12607-2022

Bogenschutz, P. A., Gettelman, A., Morrison, H., Larson, V. E., Craig, C., & Schanen, D. P. (2013). Higher-Order Turbulence Closure and Its Impact on Climate Simulations in the Community Atmosphere Model. *Journal of Climate*, *26*(23), 9655-9676 , ISSN = 0894-8755 , DOI = https //doi.org/9610.1175/jcli-d-9613-00075.00071. https://journals.ametsoc.org/view/journals/clim/26/23/jcli-d-13-00075.1.xml

Boucher, O., Randall, D., Artaxo, P., Bretherton, C., Feingold, G., Forster, P., Kerminen, V.-M., Kondo, Y., Liao, H., Lohmann, U., Rasch, P., Satheesh, S., Sherwood, S., Stevens, B., & Zhang, X. (2013). Clouds and Aerosols. In (pp. 571-892).

Chen, J., Wu, Z., Gong, X., Qiu, Y., Chen, S., Zeng, L., & Hu, M. (2024). Anthropogenic Dust as a Significant Source of Ice-Nucleating Particles in the Urban Environment. *Earth's Future*, *12*(1), e2023EF003738. https://doi.org/https://doi.org/10.1029/2023EF003738

Danabasoglu, G., Lamarque, J. F., Bacmeister, J., Bailey, D. A., DuVivier, A. K., Edwards, J., Emmons, L. K., Fasullo, J., Garcia, R., Gettelman, A., Hannay, C., Holland, M. M., Large, W. G., Lauritzen, P. H., Lawrence, D. M., Lenaerts, J. T. M., Lindsay, K., Lipscomb, W. H., Mills, M. J., . . . Strand, W. G. (2020). The Community Earth System Model Version 2 (CESM2). *Journal of Advances in Modeling Earth Systems*, *12*(2), e2019MS001916. https://agupubs.onlinelibrary.wiley.com/doi/abs/10.1029/2019MS001916

Eidhammer, T., Morrison, H., Bansemer, A., Gettelman, A., & Heymsfield, A. (2014). Comparison of ice cloud properties simulated by the Community Atmosphere Model (CAM5) with in-situ observations. *Atmospheric Chemistry & Physics*, *14*(18). https://doi.org/https://doi.org/10.5194/acp-14-10103-2014

Fan, J., Wang, Y., Rosenfeld, D., & Liu, X. (2016). Review of Aerosol-Cloud Interactions: Mechanisms, Significance and Challenges. *Journal of the Atmospheric Sciences*, *73*. https://doi.org/10.1175/JAS-D-16-0037.1

Forster, P., Storelvmo, T., Armour, K., Collins, W., Dufresne, J.-L., Frame, D., Lunt, D. J., Mauritsen, T., Palmer, M. D., Watanabe, M., Wild, M., & Zhang, H. (2023). The Earth's Energy Budget, Climate Feedbacks and Climate Sensitivity. In (pp. 923-1054). https://doi.org/10.1017/9781009157896.009

Froyd, K. D., Yu, P., Schill, G. P., Brock, C. A., Kupc, A., Williamson, C. J., Jensen, E. J., Ray, E., Rosenlof, K. H., Bian, H., Darmenov, A. S., Colarco, P. R., Diskin, G. S., Bui, T., & Murphy, D. M. (2022). Dominant role of mineral dust in cirrus cloud formation revealed by global-scale measurements. *Nature Geoscience*, *15*(3), 177-183. https://doi.org/10.1038/s41561-022-00901-w

Gasparini, B., Sullivan, S. C., Sokol, A. B., Kärcher, B., Jensen, E., & Hartmann, D. L. (2023). Opinion: Tropical cirrus – from micro-scale processes to climate-scale impacts. *Atmos. Chem. Phys.*, *23*(24), 15413-15444. https://doi.org/10.5194/acp-23-15413-2023

Gettelman, A., Liu, X., Ghan, S. J., Morrison, H., Park, S., Conley, A. J., Klein, S. A., Boyle, J., Mitchell, D. L., & Li, J.-L. F. (2010). Global simulations of ice nucleation and ice supersaturation with an improved cloud scheme in the Community Atmosphere Model. *Journal of Geophysical Research: Atmospheres*, *115*(D18). https://doi.org/https://doi.org/10.1029/2009JD013797

Gettelman, A., & Morrison, H. (2015). Advanced Two-Moment Bulk Microphysics for Global Models. Part I: Off-Line Tests and Comparison with Other Schemes. *Journal of Climate*, *28*(3), 1268-1287 , ISSN = 0894-8755 , DOI = https //doi.org/1210.1175/jcli-d-1214-00102.00101. https://journals.ametsoc.org/view/journals/clim/28/3/jcli-d-14-00102.1.xml

Glienke, S., & Mei, F. (2019). *Two-Dimensional Stereo (2D-S) Probe Instrument Handbook*. https://www.osti.gov/biblio/1597436
https://www.osti.gov/servlets/purl/1597436

Golaz, J.-C., Larson, V. E., & Cotton, W. R. (2002a). A PDF-Based Model for Boundary Layer Clouds. Part I: Method and Model Description. *Journal of the Atmospheric Sciences*, *59*(24), 3540-3551 , ISSN = 0022-4928 , DOI = https //doi.org/3510.1175/1520-0469. https://journals.ametsoc.org/view/journals/atsc/59/24/1520-0469_2002_059_3540_apbmfb_2.0.co_2.xml

Golaz, J.-C., Larson, V. E., & Cotton, W. R. (2002b). A PDF-Based Model for Boundary Layer Clouds. Part II: Model Results. *Journal of the Atmospheric Sciences*, *59*(24), 3552-3571 , ISSN = 0022-4928 , DOI = https //doi.org/3510.1175/1520-0469. https://journals.ametsoc.org/view/journals/atsc/59/24/1520-0469_2002_059_3552_apbmfb_2.0.co_2.xml

Heymsfield, A. J., Krämer, M., Luebke, A., Brown, P., Cziczo, D. J., Franklin, C., Lawson, P., Lohmann, U., McFarquhar, G., Ulanowski, Z., & Van Tricht, K. (2017). Cirrus Clouds. *Meteorological Monographs*, *58*, 2.1-2.26. https://doi.org/https://doi.org/10.1175/AMSMONOGRAPHS-D-16-0010.1

Hinz, K.-P., Kaufmann, R., & Spengler, B. (1996). Simultaneous Detection of Positive and Negative Ions From Single Airborne Particles by Real-time Laser Mass Spectrometry. *Aerosol Science and Technology*, *24*(4), 233-242. https://doi.org/10.1080/02786829608965368

Horner, G., & Gryspeerdt, E. (2023). The evolution of deep convective systems and their associated cirrus outflows. *Atmos. Chem. Phys.*, *23*(22), 14239-14253. https://doi.org/10.5194/acp-23-14239-2023

Horner, G., & Gryspeerdt, E. (2024, April 01, 2024). *How does the lifetime of cirrus detrained from deep convection impact the cloud radiative effect of the tropics?* EGU General Assembly Conference Abstracts, Vienna, Austria. https://ui.adsabs.harvard.edu/abs/2024EGUGA..2613338H

Huang, M., Xiao, H., Wang, M., & Fast, J. D. (2020). Assessing CLUBB PDF Closure Assumptions for a Continental Shallow-to-Deep Convective Transition Case Over Multiple Spatial Scales. *Journal of Advances in Modeling Earth Systems*, *12*(10), e2020MS002145. https://doi.org/https://doi.org/10.1029/2020MS002145

Iacono, M. J., Delamere, J. S., Mlawer, E. J., Shephard, M. W., Clough, S. A., & Collins, W. D. (2008). Radiative forcing by long-lived greenhouse gases: Calculations with the AER radiative transfer models. *Journal of Geophysical Research: Atmospheres*, *113*(D13). https://agupubs.onlinelibrary.wiley.com/doi/abs/10.1029/2008JD009944

Jensen, E. J., Lawson, R. P., Bergman, J. W., Pfister, L., Bui, T. P., & Schmitt, C. G. (2013). Physical processes controlling ice concentrations in synoptically forced, midlatitude cirrus. *Journal of Geophysical Research: Atmospheres*, *118*(11), 5348-5360. https://doi.org/https://doi.org/10.1002/jgrd.50421

Kärcher, B. (2022). A Parameterization of Cirrus Cloud Formation: Revisiting Competing Ice Nucleation. *Journal of Geophysical Research: Atmospheres*, *127*(18), e2022JD036907. https://doi.org/https://doi.org/10.1029/2022JD036907

Kärcher, B., DeMott, P. J., Jensen, E. J., & Harrington, J. Y. (2022). Studies on the Competition Between Homogeneous and Heterogeneous Ice Nucleation in Cirrus Formation. *Journal of Geophysical Research: Atmospheres*, *127*(3), e2021JD035805. https://doi.org/https://doi.org/10.1029/2021JD035805

Kärcher, B., Hendricks, J., & Lohmann, U. (2006). Physically based parameterization of cirrus cloud formation for use in global atmospheric models. *Journal of Geophysical Research: Atmospheres*, *111*(D1). https://doi.org/https://doi.org/10.1029/2005JD006219

Kärcher, B., & Podglajen, A. (2019). A Stochastic Representation of Temperature Fluctuations Induced by Mesoscale Gravity Waves. *Journal of Geophysical Research: Atmospheres*, *124*(21), 11506-11529. https://agupubs.onlinelibrary.wiley.com/doi/abs/10.1029/2019JD030680

Kärcher, B., & Ström, J. (2003). The roles of dynamical variability and aerosols in cirrus cloud formation. *Atmos. Chem. Phys.*, *3*(3), 823-838. https://acp.copernicus.org/articles/3/823/2003/

Knopf, D. A., & Alpert, P. A. (2023). Atmospheric ice nucleation. *Nature Reviews Physics*, *5*(4), 203-217. https://doi.org/10.1038/s42254-023-00570-7

Koop, T., Luo, B., Tsias, A., & Peter, T. (2000). Water activity as the determinant for homogeneous ice nucleation in aqueous solutions. *Nature*, *406*(6796), 611-614. https://doi.org/10.1038/35020537

Krämer, M., Rolf, C., Luebke, A., Afchine, A., Spelten, N., Costa, A., Meyer, J., Zöger, M., Smith, J., Herman, R. L., Buchholz, B., Ebert, V., Baumgardner, D., Borrmann, S., Klingebiel, M., & Avallone, L. (2016). A microphysics guide to cirrus clouds – Part 1: Cirrus types. *Atmos. Chem. Phys.*, *16*(5), 3463-3483. https://acp.copernicus.org/articles/16/3463/2016/

Krämer, M., Rolf, C., Spelten, N., Afchine, A., Fahey, D., Jensen, E., Khaykin, S., Kuhn, T., Lawson, P., Lykov, A., Pan, L. L., Riese, M., Rollins, A., Stroh, F., Thornberry, T., Wolf, V., Woods, S., Spichtinger, P., Quaas, J., & Sourdeval, O. (2020). A microphysics guide to cirrus – Part 2: Climatologies of clouds and humidity from observations. *Atmos. Chem. Phys.*, *20*(21), 12569-12608. https://acp.copernicus.org/articles/20/12569/2020/

Lawson, R. P. (2011). Effects of ice particles shattering on the 2D-S probe. *Atmos. Meas. Tech.*, *4*(7), 1361-1381. https://doi.org/https://doi.org/10.5194/amt-4-1361-2011

Lin, L., Fu, Q., Liu, X., Shan, Y., Giangrande, S. E., Elsaesser, G. S., Yang, K., & Wang, D. (2021). Improved Convective Ice Microphysics Parameterization in the NCAR CAM Model. *Journal of Geophysical Research: Atmospheres*, *126*(9), e2020JD034157. https://doi.org/https://doi.org/10.1029/2020JD034157

Lin, L., Liu, X., Zhao, X., Shan, Y., Ke, Z., Lyu, K., & Bowman, K. P. (2025). Ice nucleation by volcanic ash greatly alters cirrus cloud properties. *Science Advances*, *11*(19), eads0572. https://doi.org/doi:10.1126/sciadv.ads0572

Liou, K.-N. (1986). Influence of Cirrus Clouds on Weather and Climate Processes: A Global Perspective. *Monthly Weather Review*, *114*(6), 1167-1199. https://doi.org/10.1175/1520-0493(1986)114<1167:Ioccow>2.0.Co;2

Liu, X., Ma, P. L., Wang, H., Tilmes, S., Singh, B., Easter, R. C., Ghan, S. J., & Rasch, P. J. (2016). Description and evaluation of a new four-mode version of the Modal Aerosol Module (MAM4) within version 5.3 of the Community Atmosphere Model. *Geosci. Model Dev.*, *9*(2), 505-522. https://gmd.copernicus.org/articles/9/505/2016/

Liu, X., & Penner, J. (2005). Ice nucleation parameterization for global models. *Meteorologische Zeitschrift*, *14*, 499-514 , DOI = https //doi.org/410.1127/0941-2948/2005/0059.

Liu, X., Penner, J. E., Ghan, S. J., & Wang, M. (2007). Inclusion of ice microphysics in the NCAR Community Atmospheric Model version 3 (CAM3). *Journal of Climate*, *20*(18), 4526-4547 , ISSN = 1520-0442 , DOI = https //doi.org/4510.1175/JCLI4264.4521.

Lyu, K., Liu, X., Bacmeister, J., Zhao, X., Lin, L., Shi, Y., & Sourdeval, O. (2023). Orographic Cirrus and Its Radiative Forcing in NCAR CAM6. *Journal of Geophysical Research: Atmospheres*, *128*(10), e2022JD038164. https://agupubs.onlinelibrary.wiley.com/doi/abs/10.1029/2022JD038164

Mitchell, D. L., Garnier, A. E., & Woods, S. (2024). Advances in CALIPSO (IIR) cirrus cloud property retrievals – Part 1: Methods and testing. *EGUsphere*, *2024*, 1-44. https://doi.org/10.5194/egusphere-2024-3790

Morrison, H., & Gettelman, A. (2008). A New Two-Moment Bulk Stratiform Cloud Microphysics Scheme in the Community Atmosphere Model, Version 3 (CAM3). Part I: Description and Numerical Tests. *Journal of Climate*, *21*(15), 3642-3659 , ISSN = 0894-8755 , DOI = 3610.1175/2008jcli2105.3641. https://journals.ametsoc.org/view/journals/clim/21/15/2008jcli2105.1.xml

Muhlbauer, A., Ackerman, T. P., Comstock, J. M., Diskin, G. S., Evans, S. M., Lawson, R. P., & Marchand, R. T. (2014). Impact of large-scale dynamics on the microphysical properties of midlatitude cirrus. *Journal of Geophysical Research: Atmospheres*, *119*(7), 3976-3996. https://agupubs.onlinelibrary.wiley.com/doi/abs/10.1002/2013JD020035

Muhlbauer, A., Kalesse, H., & Kollias, P. (2014). Vertical velocities and turbulence in midlatitude anvil cirrus: A comparison between in situ aircraft measurements and ground-based Doppler cloud radar retrievals. *Geophysical Research Letters*, *41*(22), 7814-7821. https://agupubs.onlinelibrary.wiley.com/doi/abs/10.1002/2014GL062279

Muri, H., Kristjánsson, J. E., Storelvmo, T., & Pfeffer, M. A. (2014). The climatic effects of modifying cirrus clouds in a climate engineering framework. *Journal of Geophysical Research: Atmospheres*, *119*(7), 4174-4191. https://doi.org/https://doi.org/10.1002/2013JD021063

Murray, B. J., & Liu, X. (2022). Chapter 15 - Ice-nucleating particles and their effects on clouds and radiation. In K. S. Carslaw (Ed.), *Aerosols and Climate* (pp. 619-649). Elsevier. https://doi.org/https://doi.org/10.1016/B978-0-12-819766-0.00014-6

Nugent, J. M., Turbeville, S. M., Bretherton, C. S., Blossey, P. N., & Ackerman, T. P. (2022). Tropical Cirrus in Global Storm-Resolving Models: 1. Role of Deep Convection. *Earth and Space Science*, *9*(2), e2021EA001965. https://doi.org/https://doi.org/10.1029/2021EA001965

Patnaude, R., Diao, M., Liu, X., & Chu, S. (2021). Effects of thermodynamics, dynamics and aerosols on cirrus clouds based on in situ observations and NCAR CAM6. *Atmos. Chem. Phys.*, *21*(3), 1835-1859. https://acp.copernicus.org/articles/21/1835/2021/

Pruppacher, H. R., Klett, J. D., & Wang, P. K. (1998). Microphysics of clouds and precipitation. In: Taylor & Francis.

Sassen, K., & Cho, B. S. (1992). Subvisual-Thin Cirrus Lidar Dataset for Satellite Verification and Climatological Research. *Journal of Applied Meteorology and Climatology*, *31*(11), 1275-1285. https://doi.org/https://doi.org/10.1175/1520-0450(1992)031<1275:STCLDF>2.0.CO;2

Sassen, K., Wang, Z., & Liu, D. (2008). Global distribution of cirrus clouds from CloudSat/Cloud-Aerosol Lidar and Infrared Pathfinder Satellite Observations (CALIPSO) measurements. *Journal of Geophysical Research: Atmospheres*, *113*(D8). https://doi.org/https://doi.org/10.1029/2008JD009972

Shan, Y., Liu, X., Lin, L., Ke, Z., & Lu, Z. (2021). An Improved Representation of Aerosol Wet Removal by Deep Convection and Impacts on Simulated Aerosol Vertical Profiles. *Journal of Geophysical Research: Atmospheres*, *126*(13), e2020JD034173. https://agupubs.onlinelibrary.wiley.com/doi/abs/10.1029/2020JD034173

Shi, X., Liu, X., & Zhang, K. (2015). Effects of pre-existing ice crystals on cirrus clouds and comparison between different ice nucleation parameterizations with the Community Atmosphere Model (CAM5). *Atmos. Chem. Phys.*, *15*(3), 1503-1520. https://acp.copernicus.org/articles/15/1503/2015/

Song, X., & Zhang, G. J. (2011). Microphysics parameterization for convective clouds in a global climate model: Description and single-column model tests. *Journal of Geophysical Research: Atmospheres*, *116*(D2). https://doi.org/https://doi.org/10.1029/2010JD014833

Spang, R., Müller, R., & Rap, A. (2024). Radiative effect of thin cirrus clouds in the extratropical lowermost stratosphere and tropopause region. *Atmos. Chem. Phys.*, *24*(2), 1213-1230. https://doi.org/10.5194/acp-24-1213-2024

Stephens, B. B., Long, M. C., Keeling, R. F., Kort, E. A., Sweeney, C., Apel, E. C., Atlas, E. L., Beaton, S., Bent, J. D., Blake, N. J., Bresch, J. F., Casey, J., Daube, B. C., Diao, M., Diaz, E., Dierssen, H., Donets, V., Gao, B.-C., Gierach, M., . . . Watt, A. S. (2018). The O2/N2 Ratio and CO2 Airborne Southern Ocean Study. *Bulletin of the American Meteorological Society*, *99*(2), 381-402. https://doi.org/https://doi.org/10.1175/BAMS-D-16-0206.1

Tobo, Y., Adachi, K., DeMott, P., Hill, T., Hamilton, D., Mahowald, N., Nagatsuka, N., Ohata, S., Uetake, J., Kondo, Y., & Koike, M. (2019). Glacially sourced dust as a potentially significant source of ice nucleating particles. *Nature Geoscience*, *12*, 1-6. https://doi.org/10.1038/s41561-019-0314-x

Wang, P.-H., Minnis, P., McCormick, M. P., Kent, G. S., & Skeens, K. M. (1996). A 6-year climatology of cloud occurrence frequency from Stratospheric Aerosol and Gas Experiment II observations (1985–1990). *Journal of Geophysical Research: Atmospheres*, *101*(D23), 29407-29429. https://doi.org/https://doi.org/10.1029/96JD01780

Winker, D. M. P. J. C. J. A. A. S. A. C. R. J. C. P. R. F. P. F. Q. H. R. M., & Wielicki, B. A. (2010). The CALIPSO mission. *Bulletin of the American Meteorological Society*, *91(9), 1211–1230. , DOI = https://doi.org/10.1175/2010BAMS3009.1*.

Yook, S., Solomon, S., Weimer, M., Kinnison, D., Garcia, R., & Stone, K. (2025). Implementation of Sub-Grid Scale Temperature Perturbations Induced by Non-Orographic Gravity Waves in WACCM6. *Journal of Advances in Modeling Earth Systems*, *17*. https://doi.org/10.1029/2024MS004625

Zhang, G. J., & McFarlane, N. A. (1995). Sensitivity of climate simulations to the parameterization of cumulus convection in the Canadian climate centre general circulation model. *Atmosphere-Ocean*, *33*(3), 407-446. https://doi.org/10.1080/07055900.1995.9649539